First principles mechanistic study of self-limiting oxidative adsorption of remote oxygen plasma during the atomic layer deposition of alumina

doi.org/10.26434/chemrxiv.6377372.v1

First Principles Mechanistic Study of Self-Limiting Oxidative Adsorption of Remote Oxygen Plasma During the Atomic Layer Deposition of Alumina

Glen N. Fomengia, Michael Nolan, Simon D. Elliott

Submitted date: 29/05/2018 • Posted date: 30/05/2018

Citation information: Fomengia, Glen N.; Nolan, Michael; Elliott, Simon D. (2018): First Principles Mechanistic Study of Self-Limiting Oxidative Adsorption of Remote Oxygen Plasma During the Atomic Layer Deposition of Alumina. ChemRxiv. Preprint.

Plasma-enhanced atomic layer deposition (ALD) of metal oxides is a rapidly gaining interest especially in the electronics industry because of its numerous advantages over the thermal process. However, the underlying reaction mechanism is not sufficiently understood, particularly regarding saturation of the reaction and densification of the film. In this work, we employ first principles density functional theory (DFT) to determine the predominant reaction pathways, surface intermediates and by-products formed when constituents of O_2-plasma or O_3 adsorb onto a methylated surface typical of TMA-based alumina ALD. The main outcomes are that a wide variety of barrierless and highly exothermic reactions can take place. This leads to the spontaneous production of various by-products with low desorption energies and also of surface intermediates from the incomplete combustion of $-CH_3$ ligands. Surface hydroxyl groups are the most frequently observed intermediate and are formed as a consequence of the conservation of atoms and charge when methyl ligands are initially oxidized (rather than from subsequent re-adsorption of molecular water). Anionic intermediates such as formates are also commonly observed at the surface in the simulations. Formaldehyde, CH_2O, is the most frequently observed gaseous by-product. Desorption of this by-product leads to saturation of the redox reaction at the level of two singlet oxygen atoms per CH_3 group, where the oxidation state of C is zero, rather than further reaction with oxygen to higher oxidation states. We conclude that the self-limiting chemistry that defines ALD comes about in this case through the desorption by-products with partially-oxidised carbon. The simulations also show that densification occurs when ligands are removed or oxidised to intermediates, indicating that there may be an inverse relationship between Al/O coordination numbers in the final film and the concentration of chemically-bound ligands or intermediate fragments covering the surface during each ALD pulse. Therefore reactions that generate a bare surface Al will produce denser films in metal oxide ALD.

File list (2)

DFT enegetics of O plasma on methylated alumina surface... (4.40 MiB)	view on ChemRxiv	download file
Supplementary Information_O singlet paper.pdf (12.69 MiB)	view on ChemRxiv	download file

First principles mechanistic study of self-limiting oxidative adsorption of remote oxygen plasma during the atomic layer deposition of alumina

Glen N. Fomengia, Michael Nolan, Simon D. Elliott*

Glen N. Fomengia, Michael Nolan

Tyndall National Institute, University College Cork, Lee Maltings, Dyke Parade, Cork, T12 R5CP, Ireland

Simon D. Elliott

Schrödinger, 120 West 45th Street, 17th Floor, New York, NY 10036-4041, USA

*Correspondent e-mail: simon.elliott@schrodinger.com

Abstract

Plasma-enhanced atomic layer deposition (ALD) of metal oxides is a rapidly gaining interest especially in the electronics industry because of its numerous advantages over the thermal process. However, the underlying reaction mechanism is not sufficiently understood, particularly regarding saturation of the reaction and densification of the film. In this work, we employ first principles density functional theory (DFT) to determine the predominant reaction pathways, surface intermediates and by-products formed when constituents of O_2-plasma or O_3 adsorb onto a methylated surface typical of TMA-based alumina ALD. The main outcomes are that a wide variety of barrierless and highly exothermic reactions can take place. This leads to the spontaneous production of various by-products with low desorption energies and also of surface intermediates from the incomplete combustion of $–CH_3$ ligands. Surface hydroxyl groups are the most frequently observed intermediate and are formed as a consequence of the conservation of atoms and charge when methyl ligands are initially

oxidized (rather than from subsequent re-adsorption of molecular water). Anionic intermediates such as formates are also commonly observed at the surface in the simulations. Formaldehyde, CH_2O, is the most frequently observed gaseous by-product. Desorption of this by-product leads to saturation of the redox reaction at the level of two singlet oxygen atoms per CH_3 group, where the oxidation state of C is zero, rather than further reaction with oxygen to higher oxidation states. We conclude that the self-limiting chemistry that defines ALD comes about in this case through the desorption by-products with partially-oxidised carbon. The simulations also show that densification occurs when ligands are removed or oxidised to intermediates, indicating that there may be an inverse relationship between Al/O coordination numbers in the final film and the concentration of chemically-bound ligands or intermediate fragments covering the surface during each ALD pulse. Therefore reactions that generate a bare surface Al will produce denser films in metal oxide ALD.

1. Introduction

Atomic layer deposition is an unrivalled vapour technique for the deposition of thin films at the nanoscale from precursor chemicals and has many technological applications, especially in the electronics industry where it enables the continuous down scaling of devices.[1] While thermal ALD has been the traditional method for depositing these films, in many cases it is not possible or desirable to operate at temperatures high enough to activate the precursors and unwanted side reactions may occur, leading to impurities deposited in the film or low film uniformity. Plasma ALD is one way of overcoming this limitation: short plasma pulses introduce active species such as radicals and ions that can quickly undergo reactions at the surface, allowing the growth of high quality films at a lower overall temperature.[2] More so, their high reactivity makes it even more energetically efficient in removing ligands compared to the thermal process.

Plasma ALD can have other advantages over the thermal process. The deposited films often show improved material properties relative to those from comparable thermal vapour techniques. For instance, the resistivity of TiN film deposited from $TiCl_4$ and H_2-N_2 plasma is significantly lower than that of a film grown from the thermal process with NH_3, even at a lower substrate temperature of 100 °C.[3][4] O_2 plasma is a useful alternative to H_2O as an O source in ALD. H_2O tends to stick to the walls of the reactor and desorb slowly, even during the metal precursor pulse, unless very long purge times are used.[5] O_2 plasma does not stick and can thus improve throughput and reduce side reactions.[6][7] Further efficiencies can be obtained by using the same gas as both the plasma source gas and purge gas via turning the plasma on and off, especially at low temperatures where the gas is unreactive with the co-reagent, film and by-products. This has been reported for Al_2O_3[7], HfO_2 from $Hf[N(C_2H_5)(CH_3)]_5$ and Ta_2O_5 from $Ta[N(CH_3)_2]_5$ using O_2 as both plasma and purge gas.[8]

Furthermore, doping of low concentrations of N atoms into oxides using a mixture of N_2-O_2 as plasma source has been achieved. Film stoichiometry can be controlled by changing the plasma composition and exposure time, opening up the possibility of tuning material properties.

The production of highly dense, conformal and high quality Al_2O_3 films is desirable for diverse applications such as in electronic devices, as good moisture permeation barriers for packaging in organic light emitting devices (OLED), and in photonics and photovoltaics.[3,9] The thermal ALD of alumina from trimethylaluminium (TMA) and H_2O has been well been investigated both theoretically and experimentally, making it a prototypical process for understanding ALD mechanisms.[10–13] Many experimental papers have also been published for the corresponding plasma process using TMA+O_2-plasma.[2, 7,14–18] In some cases, better film properties (density, refractive index, electrical resistivity) are obtained for the O_2 plasma process relative to the H_2O process[5,18–20], making the plasma process useful for the numerous applications outlined above. Ozone (O_3) has also been systematically studied as another oxygen source for alumina ALD and can be considered as similar in many ways to the O_2 plasma process.[21] However, these experiments show that at low temperatures such as 70 °C, the O_3 process produces less dense and poor conformal films compared to H_2O and O_2 plasma processes. In addition, lower growth rates of 1.1 Å/cycle at 70 °C have been obtained for the O_3 process when compared to O_2 plasma (1.8 Å/cycle).[22] Nevertheless, under identical deposition temperature, the ozone process gives a higher growth rate than the H_2O process (0.8 Å/cycle).[19]

However the mechanism of plasma or ozone-based ALD of alumina is not as well established as that of the H_2O-based process. The detection of CH_4 as a by-product during the TMA pulse[23] indicates that an OH-covered surface exists at the end of the plasma pulse. It has

often been suggested that OH is regenerated during the plasma step by the dissociative adsorption of H_2O on the surface,[23,24] where H_2O is a possible product of oxidation of the CH_3 ligands on the surface by the incident plasma.[21] An alternative source of OH is proposed from density functional theory (DFT) calculations that show OH groups being produced directly on the surface when CH_3 groups of the ligands are oxidized[21]. This study also proposed that C_2H_4 can be formed as by-product through association of the resulting CH_2 groups via a triplet transition state.

In another study, *in situ* FTIR (Fourier-transform infrared spectroscopy) combined with DFT band assignments indicated the presence of formate, -OCHO, when O_3 interacted with methylated-Al_2O_3, along with decomposition of formate to CO and surf-OH at higher temperatures.[24]

Clearly, many open questions remain about the mechanism of the surface reactions of O_2 plasma or O_3 during oxide ALD. In this paper we employ DFT to determine the predominant reaction pathways, surface intermediates and by-products formed when constituents of O_2-plasma or O_3 adsorb onto a methylated surface typical of TMA-based alumina ALD. Given that the self-limiting chemistry is the defining characteristic of ALD, we are particularly interested in which reactions self-limit through kinetics and which reactions are spontaneous, but self-limit through reactants becoming exhausted. Our study is confined to C-containing by-products that desorb as a direct result of the oxidative adsorption of plasma species; consideration of slower reactions that may occur between surface intermediates is outside the scope of this study.

Based on the energetics calculated using DFT in this paper, we predict new reaction pathways for the regeneration of surface OH groups and new surface intermediates, together

with mechanisms leading to densification, in addition to confirming the production of the formates, bicarbonates and carbonates observed by experiments[25,26].

The atoms in a precursor gas or at the surface are generally characterised by lower coordination numbers than the same atoms in a bulk solid. The term densification is used to describe the increase in coordination number of atoms in the adsorbate or at the surface as reactions occur that make them more bulk-like. Simulations indicate that densification is an important part of the mechanism of oxide ALD[27,28] and in this study we also discuss how the chemistry of the plasma pulse affects whether Al and O densify and adopt a coordination environment that can be related to a bulk phase.

It has frequently been observed that hydroxylation of alumina plays an important role in its ALD surface reactions. For instance, the growth per cycle of Al_2O_3 is linearly dependent on the degree of hydroxylation of the surface.[29] The maximum hydroxylation was modelled by Elliott *et al.* by using a gibbsite-like surface, neglecting finite temperature effects.[12] More realistic conditions were taken into account by Łodziana *et al.*, who computed that the most favourable OH termination under low pressure (P = 2 Pa) and typical experimental temperature (T = 450 K) features two types of OH groups, here termed lower and higher OH groups.[30] This surface model has been used by T. Weckman and K. Laasonen to predict reaction pathways for the TMA pulse during the ALD of alumina.[11] We have reproduced and used this model in answering some of these new questions to refine our view of ALD surface chemistry.

A commonly used configuration is the remote plasma ALD reactor where plasma species are generated in the inductively coupled plasma (ICP) configuration. One major advantage is its wide range of operating pressures (1-1000 mTorr).[23] The ICP source powered at 100-600 W produces a high electron temperature of approximately 3.5 x 10^4 K, corresponding to a mean

kinetic energy of the electrons of about 3 eV. These hot electrons can ionize and excite gaseous species through electron impact collisions, but with a negligible amount of heat being transferred from the electrons to the heavier gas phase species. As a result, the temperature of the gaseous ions, atoms and molecules in the plasma is low (300-500 K)[2] and it is termed a 'cold' plasma. The degree of ionization in cold plasmas is also typically low, ranging 10^{-6} to 10^{-3} depending on reactor geometry, and so relatively few ions arrive at the substrate compared to neutral radicals, atoms and molecules. The proportion of charged species incident on the substrate can however be increased by substrate or electrode biasing.[31]

The reactive species in O_2-plasma has been characterized by modelling the plasma discharge in the ICP configuration as consisting of triplet molecules, $^3O_2$; singlet molecules, $^1O_2$; triplet atoms, ^3O; singlet atoms, ^1O; molecule cations, O_2^+; atom cations, O^+; atom anions, O^-; and electrons (e), as well as accompanying radiation.[2,32][33][34] In the remote plasma ALD configuration in the absence of substrate biasing, it has been shown that the predominant species reaching the surface are ^1O, ^3O, $^1O_2$ and $^3O_2$. Therefore, in this report we calculate only reactions of ^1O atoms. ^1O atoms are also expected to be the predominant active species from thermal dissociation of ozone.[21,23] Simulating the remaining radicals and molecules of the remote plasma will be reported in a follow-up publication.

2. Methods and Model

DFT is used to model the ALD of Al_2O_3 from TMA and ^1O atoms (from O_2 plasma or ozone) based on its reliability to compute properties of materials like atomic structure and reaction energetics. 3D-periodic boundary conditions are imposed, so that the surface is modelled by an infinite series of stacked slabs, separated by a vacuum. We employ the Vienna ab initio simulation package (VASP, version 5.3)[35] with the following technical parameters: plane wave basis to a cutoff of 400 eV, Perdew-Burke-Ernzerhof (PBE) density functional[36] coupled with projector augmented-wave (PAW)[37] pseudopotential descriptors for the effect of core electrons, the valence electronic configurations for Al, O, C and H were $[Ne]s^2p^1$, $[He]s^2p^4$, $[He]s^2p^2$, and s^1 respectively, sparse sampling of the reciprocal space using 3×3×3 and 3×3×1 Monkhorst-Pack k-point grids[38] for bulk and surface calculations respectively, with gamma-point only sampling for gas-phase molecules and atoms, Gaussian smearing with width set to 0.2 eV, medium grid for FFT mesh for surface calculations and self-consistent electronic steps converged to 10^{-3} eV.

A six layer (13 Å) thick slab of α-Al_2O_3 was generated so as to give the Al terminated (0 0 0 1) bare surface that is considered to be the most stable.[39] Each crystalline slab was separated by vacuum of 14 Å thickness. Convergence of the slab with respect to vacuum thickness, k-point sampling and slab thickness was ensured. A 2×2 slab (of surface area 0.80 nm^2) was used so as to minimize intercell image interactions and maximize relaxation of the adsorbate. All atoms within the slab were allowed to relax without any constraints imposed on them until gradients were less than 0.03 eV/Å.

Figure 1 right panel (**A**) shows a structure for the hydroxylated α-Al_2O_3 surface under realistic ALD conditions of pressure P = 2 Pa of H_2O and temperature T = 450 K, as

proposed by Z. Łodziana *et al.*[30]. It is observed that under such conditions, water molecules dissociate on bare Al and O to introduce two types of hydroxyl groups on the surface: capping (lower) and terminal (upper). This substrate model was used by T. Weckman and K. Laasonen as the surface model in DFT calculations of TMA adsorption during ALD and was found to have a considerable effect on the reaction mechanisms and energetics.[11] Our computed reaction energy for the dissociative adsorption of a water molecule on the bare α-Al_2O_3 surface is -1.48 eV per molecule (Table 1, reaction **A**), in agreement with the value they obtained (-1.49 eV corresponding to one monolayer water coverage). We have reproduced and used this hydroxylated surface model as the starting point for studying the ALD growth pathways of α-Al_2O_3 from TMA and O_2 plasma. The model contains 4 upper and 4 lower OH groups per 2×2 cell.

We are interested in finding likely surface intermediates and gas-phase by-products. Hence we try many different initial positions and concentrations of ^1O atoms interacting with the methylated surface. Previous DFT studies of ALD mechanism have (of necessity) typically considered the reaction of a single precursor or reagent with a single adsorbate in a small simulation cell.[13] As a result, little could be determined about structures formed between multiple reacted adsorbates. Instead, here, we use a relatively large model of the methylated surface featuring a range of adsorbate geometries, and we introduce multiple ^1O atoms simultaneously so as to describe a range of plasma concentrations. These initial geometries are presented in the supplementary information (S. I.). We use geometry optimisations to show the products of barrierless reactions. No activation energies for subsequent reactions are calculated, with the exception of the energy cost of by-product desorption.

All energetics are quoted at T=0 K with no zero point correction. Reference energies of gas phase atoms and molecules were calculated in a cubic cell of side 20 Å. All the reaction

energies during adsorption of ^1O atoms on the methylated surface were computed relative to gas-phase ^1O because of deficiencies in the treatment of O_2 by DFT.[21]

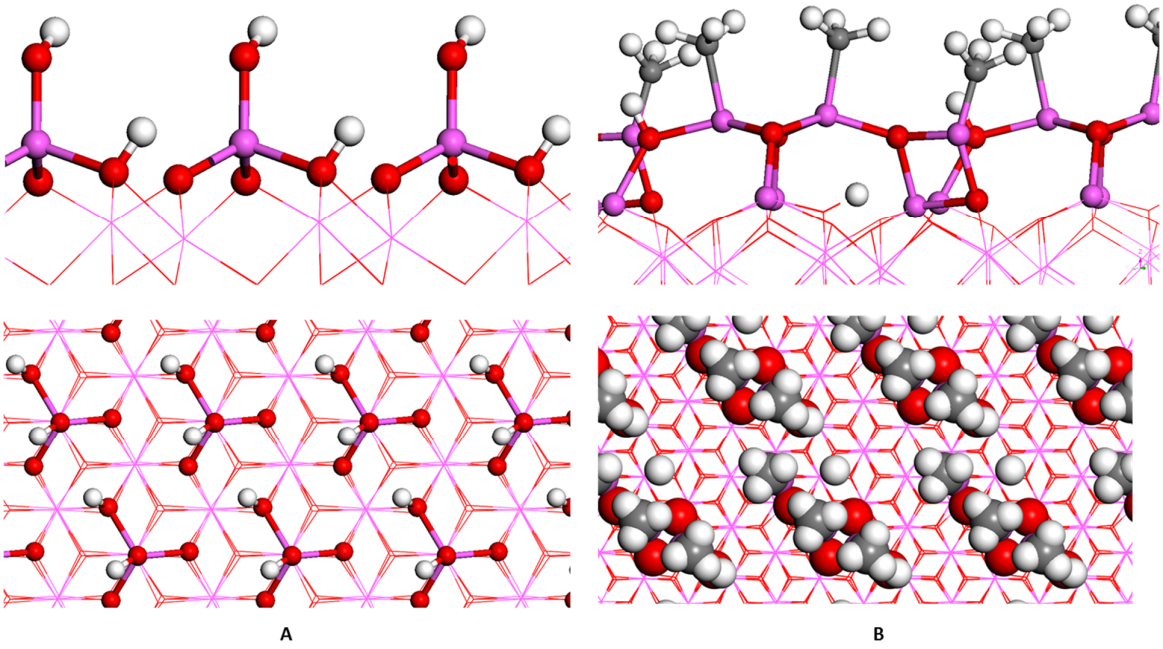

Figure 1: The left panel (A) shows side and top views of the hydroxylated 2×2 (0001) α-Al_2O_3 surface formed from dissociatively adsorbed water as described by Z. Łodziana *et al.* [34]. The surface is terminated by two types of hydroxyl groups: lower-OH (capping) and higher-OH (terminal). A monolayer coverage of -OH groups is obtained when four water molecules adsorb onto the 2×2 cell with a surface area of 0.80 nm^2. The right panel (B) shows side and top views of the optimised methylated 2×2 (0001) α-Al_2O_3 surface after hydroxylation and then saturation with TMA, denoted MS. The lines indicate the initial bonds of the (0 0 0 1) Al_2O_3 substrate and balls show surface atoms. Red = O, Purple = Al, White = H, Grey = C.

3. Results

3.1 TMA pulse

We initially developed a model of the methylated surface denoted **MS** (Figure 1), by taking into account previous calculations that investigate TMA adsorption on an Al_2O_3 substrate.[12,40] The widely adopted mechanism is that TMA chemisorbs via Lewis acidic Al on available oxygen Lewis basic sites of the substrate and that up to two CH_3 ligands per TMA desorb as CH_4, each through proton transfer from the surface to the absorbate over a reaction barrier.

The degree of saturation is controlled by the bulky nature of the adsorbed TMA fragments and the availability of electron-rich Lewis basic sites for TMA chemisorption. Previous DFT calculations[12] have shown that TMA molecules intially adsorb on the unbridged (higher) surface OH groups of the hydroxylated surface model. The vertical orientation of these OH groups prevents TMA adsorption on the lower OH groups. Some studies have observed a mixed surface of monomethylaluminium ($AlCH_3$) and dimethylaluminium ($Al(CH_3)_2$),[41][42] while others report surfaces covered only with $AlCH_3$ fragments.[29] The latter was chosen for this work as the most straightforward starting point to study the complexities of plasma surface reactions. Eventually, the results obtained from this simplified $AlCH_3$ surface will in the future help us to investigate the more complicated mixed surface.

Therefore, to get a methylated surface model that is close to saturation with respect to TMA without repeating these calculation steps, we systematically removed at each stage two CH_4 molecules from each TMA adsorbed on oxygen sites, to yield an $Al(CH_3)$ fragment. After geometry optimisation and calculation of the reaction energy relative to gas-phase TMA, the

process of adsorbing $Al(CH_3)$ was repeated until the near-ideal saturated surface shown in Figure 1 right panel (**B**) was obtained.

As CH_4 molecules are eliminated, steric effects reduce, oxygen Lewis basic sites become available, and further TMA molecules are adsorbed. This continues until the adsorption reaction self-limits by loss of basicity of surface oxygen partially due to steric crowding.[28] We estimate using DFT that saturation occurs in this case at a coverage of about 3 ($AlCH_3$) per 2×2 cell (0.27 CH_3/nm^2) as this gives the most exothermic reaction energy of -5.26 eV per TMA (Table 1, **B)**. Chemisorption of a fourth TMA in this cell appears to be unlikely since, after loss of $2CH_4$, the overall reaction energy is lower in magnitude than that of the third TMA (Table 1, reaction **B***) indicating the onset of energetically unfavourable steric repulsion between the four $AlCH_3$ fragments in the cell (see S. I. B1).

Improved packing in a larger simulation cell would presumably yield an even greater exothermicity at an optimum coverage slightly greater than 0.27 CH_3/nm^2. On the other hand, entropy and immobile ligands argue for the experimental coverage reaching equilibrium at slightly less than the optimum. We therefore suggest that the methylated surface with 3($AlCH_3$) and 2(OH) per cell, denoted **MS** (Figure 1, right panel), is a realistic model and it has been used in the rest of this paper to investigate the reaction mechanism with different initial positions and concentrations of ^1O atom during the O-plasma step of the ALD process.

Table 1: H_2O (A) and TMA (B) reaction energies for adsorption, dissociation and possibly by-product desorption on bare and hydroxylated α- Al_2O_3 surface respectively. The formula of the 2×2 cell of α-Al_2O_3 slab is $(Al_2O_3)_{24}$. The surface is denoted as |--.

A	$\|\text{--}(Al_2O_3)_2 + 4H_2O \rightarrow \|\text{--}O_2\text{-}(HO)_4(AlOH)_4$	-1.48 eV/H_2O
B	$8\|\text{--}OH + 3Al(CH_3)_3 \rightarrow \|\text{--}O_6\text{-}(HO)(AlCH_3)_3 + 6CH_4 + \|\text{--}OH$	-5.26 eV/TMA
B*	$8\|\text{--}OH + 4Al(CH_3)_3 \rightarrow \|\text{--}O_8\text{-}(AlCH_3)_4 + 8CH_4$	-2.88 eV/TMA

3.2 Oxygen plasma pulse

The aim is to look at how ^1O plasma interacts with the **MS** surface. Different concentrations of ^1O atoms were computed within the 2×2 **MS** cell and the results are presented below and in Table 2. We have undertaken many relaxations with each concentration of ^1O and some starting geometries and less stable relaxed geometries are shown in the SI. Given the high computational load in examining multiple starting geometries, we have examined a limited, but representative, set of singlet oxygen starting configurations at each concentration.

These results are grouped into subsections based on the occurrence of similar by-products and surface intermediates as described below.

3.2.1 Formation of CH_2O as by-product

This section presents results when CH_2O is spontaneously produced as the main by-product during reactions of **MS** with ^1O atoms.

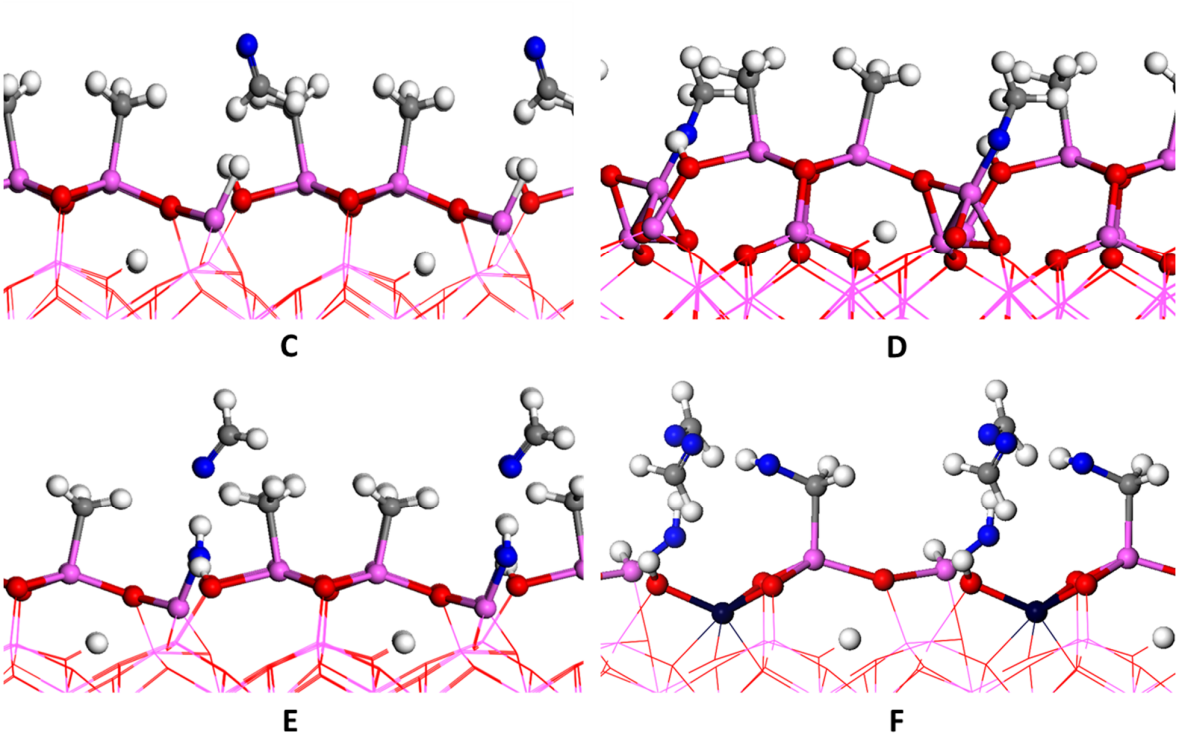

Figure 2: Optimized geometry of surface models showing the formation of CH_2O as principal by-product after the oxidation of methyl groups of MS with different density of ^1O atoms. Blue = introduced ^1O; Black = densified Al.

Initially, a single ^1O atom approaching the upper surface of **MS** from above is observed during the geometry optimisation to oxidize the methyl ligand spontaneously, producing CH_2O as by-product (see Figure 2, **C**). The reaction is exothermic with a reaction energy relative to **MS** and the isolated ^1O atom of -4.99 eV produced when the atom approaches from the top of the simulation cell (Table 2, reaction **C**). Desorption of the CH_2O by-product (computed by removing it from the simulation cell) costs 0.05 eV at 0 K and so is likely to be thermodynamically favoured at typical experimental temperatures. Simultaneously, H^- formed from the dissociation of the ligand binds with the Al whose ligand is oxidized. This diffusion is also observed in some reactions of **MS** with 4^1O (**G**) and 7^1O (**L**) below.

Table 2: Computed DFT reaction energies for O singlet atoms on methylated α-Al2O3 2×2 surface (MS). The reported desorption energy of by-products listed here is the total for all the different by-product molecules per cell produced in each reaction. Σ*Q*(C) is the sum of the formal oxidation states of C atoms per cell based on the values in Table 4.

	Reaction	Reaction energy (eV per ^{1}O)	Desorption energy of by-products (eV per cell)	Σ*Q*(C) in surface-bound products	Σ*Q*(C) in gaseous by-products	Structure
C	$\|\text{--}(AlCH_3)_3 + {}^1O \rightarrow \|\text{--}(AlCH_3)_2 + \|\text{--}AlH + CH_2O$	-4.99	0.05	-8	0	Figure 2
D	$\|\text{--}(AlCH_3)_3 + {}^1O \rightarrow \|\text{--}(AlCH_3)_2 + \|\text{--}AlOCH_3$	-7.37	n/a	-10	n/a	Figure 2
E	$\|\text{--}(AlCH_3)_3 + 2{}^1O \rightarrow \|\text{--}(AlCH_3)_2 + \|\text{--}AlOH + CH_2O$	-6.76	0.28	-8	0	Figure 2
F	$\|\text{--}(AlCH_3)_3 + 4{}^1O \rightarrow \|\text{--}AlOH + \|\text{--}AlH + \|\text{--}AlCH_2OH + 2CH_2O$	-6.39	0.34	-2	0	Figure 2
H	$\|\text{--}(AlCH_3)_3 + 4{}^1O \rightarrow \|\text{--}Al(CH_3)_2 + \|\text{--}Al_2OCHO + H_2O_2$	-5.84	0.72	-6	n/a	Figure 3
I	$\|\text{--}(AlCH_3)_3 + 5{}^1O \rightarrow \|\text{--}AlOH + \|\text{--}AlOCH_2 + \|\text{--}AlO + CH_3OCH_2OH$	-6.96	0.95	0	-1	Figure 5
J	$\|\text{--}O\text{-}(AlCH_3)_3 + 6{}^1O \rightarrow \|\text{--}AlOH + \|\text{--}AlO_2CH_2 + \|\text{--}AlOCHO + \|\text{--}OH + CH_3OH$	-7.35	0.55	+2	-2	Figure 4
K	$\|\text{--}(AlCH_3)_3 + 6{}^1O \rightarrow \|\text{--}AlOAlOH + \|\text{--}AlOHCH_2OH + 2CH_2O$	-6.91	0.68	0	0	Figure 4
L	$\|\text{--}(AlCH_3)_3 + 7{}^1O \rightarrow \|\text{--}AlCH_3 + \|\text{--}AlCH_2(O_2)H + \|\text{--}AlCHO + O_2 + H_2O_2$	-4.67	0.41	-6	n/a	Figure 5
M	$\|\text{--}(AlCH_3)_3 + 8{}^1O \rightarrow \|\text{--}OH(AlOCHO)_2 + \|\text{--}AlOHCH_2OH + H_2O$	-7.12	0.28	+4	n/a	Figure 5
O	$\|\text{--}(AlCH_3)_3 + 10{}^1O \rightarrow \|\text{--}AlOH + \|\text{--}Al[HCO_3] + \|\text{--}Al[HCO_2(O_2)] + CO + H_2O + 2H_2$	-6.55	0.60	+8	+2	Figure 3

We also investigated an alternative initial geometry where ^1O approaches surface Al rather than CH_3^- and the products are shown in Figure 2, **D**. In this case, ^1O spontaneously inserts into the Al-C bond to form a methoxyl ligand, $AlOCH_3$, with reaction energy of -7.37 eV (Table 2, reaction **D**). Such a mechanism was first proposed by Prechtl *et al.*[43] and also observed in calculations by Elliott *et al.*[21] No densification of Al atoms and no gas-phase by-products are produced spontaneously at this point.

We suggest that this reaction pathway takes place in environments where Al is under coordinated ($\leq$3 bonds) and the pressure of incident ^1O is low. To test this assumption, the 4-coordinated Al at the surface was allowed to interact with ^1O. This resulted in no insertion of ^1O into Al-C, rather forming adsorbed peroxide (*i.e.* $(O_2)^{2-}$ with computed O-O bond length = 1.53 Å) in one case and bridged to Al in the bulk (Al-O-Al) in the other case (see S. I., structures A1and A2). The reaction energies of -3.64 eV and -3.81 eV respectively indicate that these reactions are about half as exothermic as the insertion case.

Another computed geometry was considered with the ^1O atom initially placed in various positions in the subsurface layer. In one case the atom moved out of the subsurface layer and reacted with pre-existing oxygen at the alumina surface to form peroxide with O-O bond length of 1.53 Å. The reaction energy is just -3.63 eV/^1O (see S. I, structure A3). In the other reaction, the subsurface ^1O formed an $-OCH_3$ fragment by accepting a $-CH_3$ ligand from Al above (see S. I., structure A4). Meanwhile this Al without its ligand sank into the subsurface, thereby staying 4-coordinated. The reaction energy released is -7.68 eV/^1O in good close agreement with the geometry where insertion spontaneously occurred (Table 2, reaction **D**).

Increasing the ^1O concentration to two atoms per cell produced a new set of results as seen in Figure 2, **E**. The barrierless and exothermic reaction showed a reaction energy of -6.76 eV per ^1O (see Table 2, **E)**. One of the ^1O oxidized the methyl ligand to spontaneously form CH-

$_2$O, which could be desorbed from the simulation cell at a cost of 0.28 eV. The other ^{1}O formed an OH fragment with the Al that lost its ligand. This represents the completion of reaction **D** with one ^{1}O, since the Al-H product of that reaction can evidently combine with the extra ^{1}O to form Al-OH here in reaction **E**. The surface Al thus remains 4-coordinated after the reaction.

We introduced three ^{1}O atoms above the CH_3 ligands and one ^{1}O atom to the side of one Al of the **MS** cell and observed the reactions that took place spontaneously during geometry optimisation (reaction **F** in Table 2 and Figure 2). One ^{1}O inserted into a C-H bond to yield the alcohol $AlCH_2OH$, as previously computed by Elliott *et al.*[4]Another $Al(CH_3)$ fragment, with initially 4-coordinate Al, donated CH_2 to one ^{1}O for oxidation to CH_2O and H^- to another ^{1}O to form surface OH, which is the same as reaction **E**. This loss of a ligand allowed the Al atom to densify into the slab, bond to subsurface O and become 6-coordinated. The third $Al(CH_3)$ fragment also reacted to yield CH_2O, but this time the remaining H bonded to the Al, presumably as hydride H^- (Al-H bond length of 1.614 Å), with Al remaining 4-coordinated and this matches reaction **C**. The total reaction energy for all these reactions together in the slab was -6.39 eV per ^{1}O. Desorbing the loosely-bound CH_2O by-products was computed to cost 0.34 eV per CH_2O.

Short DFT-based MD simulations from the same initial geometry as **F** at 423 K spontaneously produced the same by-products and surface fragments. However, in MD, H^- that was weakly bonded to Al combined with a nearby proton in the subsurface layer to produce H_2 (see S. I. structure F2). This supports our finding that Al-H in reaction **C** is metastable relative to further oxidation in **D**.

3.2.2 Formation of alcohol by-products and intermediates

Having observed the formation of the monoalcohol surf-CH_2OH intermediate in reaction **F**, the stability of multiple alcohol units was investigated by manually inserting ^1O atoms into all C-H bonds of one or more $–CH_3$ groups (Figure 3). The resulting $–C(OH)_x$ intermediates were observed to be unstable. For instance, inserting three ^1O into adjacent C-H bonds gave a spontaneous reaction during optimisation with the release of -5.84 eV per cell to form H_2O_2 as by-product (Table 2, Reaction **H**).

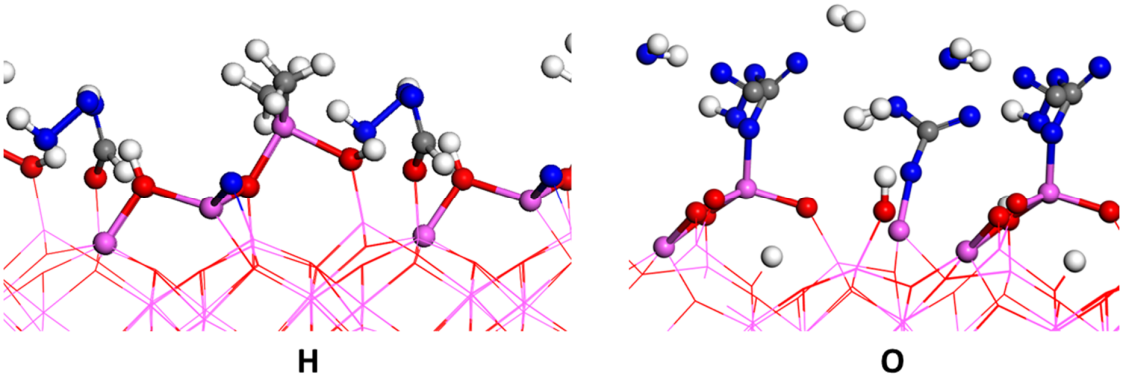

Figure 3: Surface products formed after geometry optimisation of MS with ^1O (reaction H and O) where initial $AlC(OH)_x$ geometries were generated by inserting the singlet atoms into multiple C-H bonds. Left panel (H): reaction of MS with three ^1O atoms forming $Al(CH_3)_2$ and AlOCHO as fragments and H_2O_2 as by-product. Right panel (O): reaction of MS with nine ^1O atoms. Surface fragments are OH, $Al[HCO_2(O_2)]$ and -$Al[HCO_3]$, while H_2O, two H_2 and CO are spontaneously formed as by-products.

In addition, an unreacted proton from the subsurface migrated to the surface to form another bridged OH group. Desorption of the H_2O_2 by-product costs 0.72 eV, leaving -$Al(CH_3)_2$ and formate, -Al(OCHO)[24], as surface fragments.

We also investigated the extreme case where nine ^1O atoms were inserted by hand into all C-H bonds prior to optimisation (Figure 3, **O**). This configuration was also found to be unstable with a reaction energy of -6.55 eV/^1O (Table 2, reaction **O**). The by-products spontaneously produced in this case are H_2, H_2O and CO which were all removed from the simulation cell at a total cost of 0.60 eV. The remaining surface fragments are hydrogencarbonate -$Al[HCO_3]$,

a peroxide version of hydrogencarbonate -Al[$CO_2(O_2)H$] and hydroxyl -OH. One Al densified to become 5-coordinated while the other two remained 4-coordinated.

3.2.3 Reaction of MS with six ^{1}O atoms

We are interested to see if reaction **E** is likely to occur at all CH_3 groups simultaneously, that is, whether introducing six ^{1}O per cell will produce three CH_2O by-products and three surface hydroxyl groups. Clearly there are many possible configurations for six ^{1}O per cell (as there are for all the other simulations) and selected simulations are presented below.

Reaction **J** in Figure 4 and Table 2 shows the spontaneous reaction between 6 ^{1}O atoms and the methylated surface, which is exothermic with ΔE=-7.35 eV/^{1}O. The starting configuration is such that half of these singlet atoms attack –CH_3 ligands from the top while the rest attack surface Al. Oxidation spontaneously produces methanol, CH_3OH, as by-product with a rather high desorption energy of 0.55 eV. Surface fragments consist of two –OH, –Al(OCHO) and –AlO_2CH_2 intermediates after desorption of methanol. After geometry optimisation, one surface Al densifies from 4- to 5-coordinated, another Al stays 4-coordinated, while the last Al changes from 3- to 4-coordinated. DFT-based MD simulations from the same initial geometry produced different surface fragments including hydride binding to Al, which densifies to 6 coordination following desorption of the MD by-products CH_2O and HCOOH (Optimised geometry in S. I. structure J2).

DFT optimisation involving 6 ^{1}O atoms with MS in different initial positions produced a new set of by-products (reaction **K** in Figure 4 and Table 2). When two ^{1}O atoms were placed near each $AlCH_3$ surface fragment, geometry optimisation revealed a barrierless reaction that released -6.91 eV/^{1}O and spontaneously produced two CH_2O molecules. The surface intermediates were –OH, bridging-O^{2-} and methanediol $CH_2(OH)_2$, with the latter bound to the surface via Al-O of 1.92 Å.

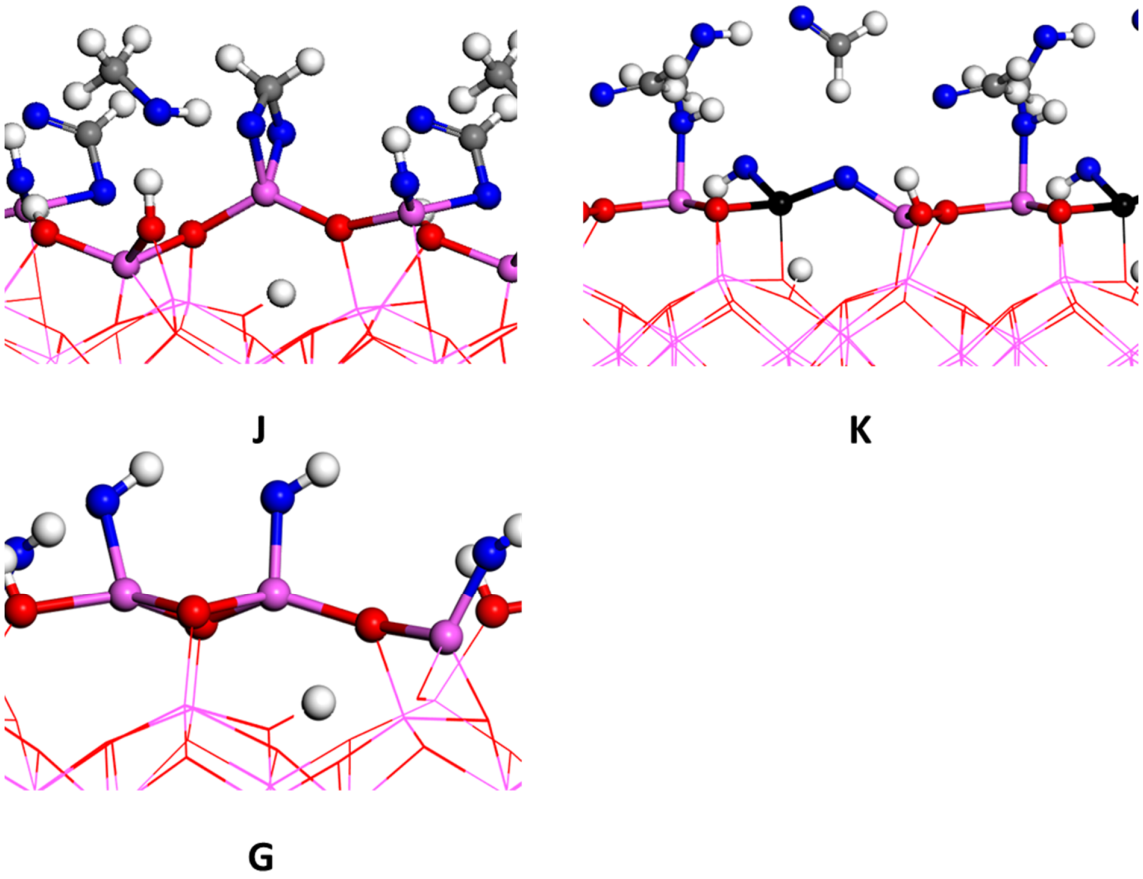

Figure 4: Reaction products after geometry optimisation of MS with various orientations of six ^{1}O atoms per cell, *i.e.* two ^{1}O per CH_3 group. In J, CH_3OH is the by-product and surface intermediates are -AlO_yCH_x- and –OH groups. In K, the by-products are $2CH_2O$ while -$AlOHCH_2OH$ and –OH are surface fragments. In G we assumed that all ligands are oxidized to form three CH_2O that after desorption leave –OH fragments at the surface.

The desorption energy per CH_2O molecule is computed to be 0.34 eV and relatively low compared to previous calculation when CH_3OH is formed. An increase in coordination from 3 to 4 is observed for one Al while the other two Al stay 4-coordinated.

Observing the formation of CH_2O as by-product in most the reactions prompted us to investigate the case where all three ligands were oxidized by six ^{1}O atoms to $3OH+3CH_2O$, with the latter removed from the simulation cell so as to leave the surface terminated by OH groups, a total of five OH per cell (Figure 4, **G**). The total reaction energy after desorption is

computed to be -6.61 eV/^{1}O (Table 3). All the surface Al stay 4-coordinated and there is no densification into the subsurface layer, apparently because all Al are bonded to OH groups.

3.1.1 Reaction of MS with high ^{1}O concentrations

We now present the reactions that result from high concentrations of ^{1}O, between five and ten ^{1}O simultaneously delivered to the **MS** cell.

Reaction **I** (Figure 5 and Table 2) shows that five ^{1}O atoms per cell undergo a barrierless reaction with **MS** to spontaneously produce CH_3OCH_2OH as by-product. It was observed that three ^{1}O and two CH_3 were involved in forming this by-product and a bridging oxide anion, -Al-O-Al-. The remaining $–CH_3$ reacted with two ^{1}O atoms in the same manner as reaction **E**, forming an OH fragment and CH_2O, but with the latter bound to under-coordinated surface Al (Al-O bond length of 2.02 Å). This combination of reactions is exothermic releasing -6.92 eV per ^{1}O. The desorption energy of the ostensibly neutral by-product CH_3OCH_2OH is 0.95 eV, suggesting that it persists as a surface-bound intermediate. After the barrierless reaction, the coordination number of two Al at the surface increases by one from three to four-one densifies into the subsurface layer after loss of its ligand, while the other Al becomes 5-coordinated after the loss of its ligand**.**

With more O present in the system, different by-products are spontaneously produced as seen for seven ^{1}O per cell (reaction **L** in Figure 5 and Table 2). The reaction is exothermic, but significantly less so than the other reactions, releasing just -4.67 eV/^{1}O. Two ^{1}O atoms recombine to form O_2 gas, and two others produce H_2O_2, which may both be desorbed from the system at a total cost of 0.41 eV. This suggests that recombination into O_2 and $(O_2)^{2-}$ is a kinetically viable route at this density of ^{1}O atoms, rather than further oxidation of surface C,

which would be more thermodynamically favoured. One surface fragment formed is -AlOCH, which can be tentatively described as deprotonated CH_2O.

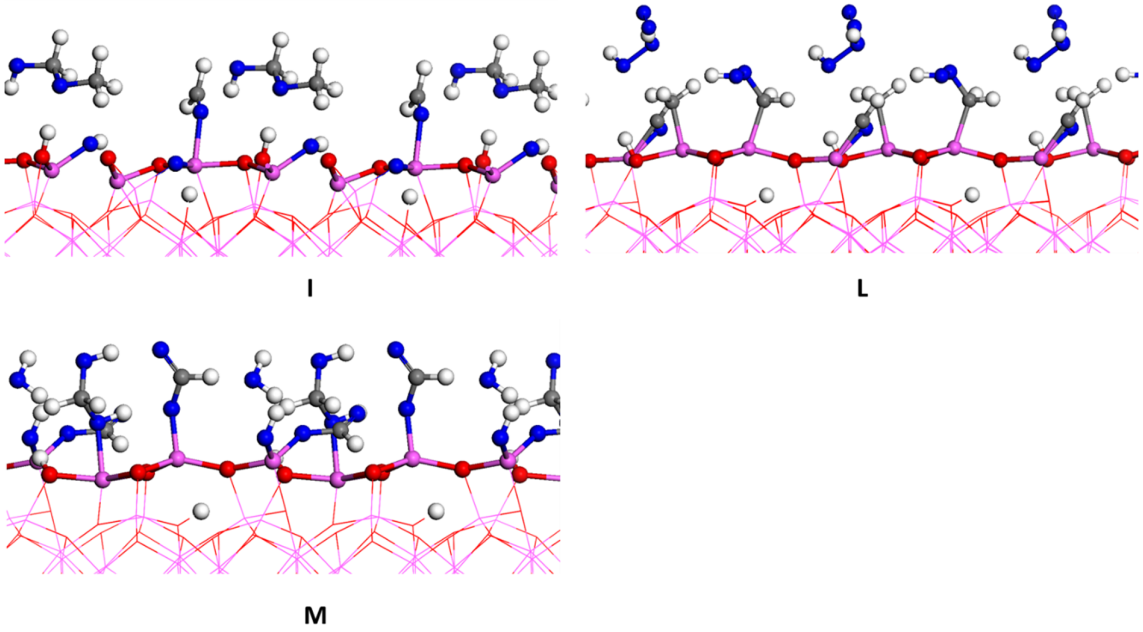

Figure 5: Surface models after geometry optimisation of MS with high concentrations of ^1O. In I, MS reacts with five ^1O atoms and CH_3OCH_2OH is formed as by-product, surface fragments are $–AlOCH_2$ and –OH, and bridging O. In L, MS reacted with seven ^1O atoms to give H_2O_2 and O_2 as by-products along with surface intermediates $–AlCH_2(O_2)H$, $-AlCH_3$ and –AlOCH. In M, eight ^1O atoms produce H_2O and two formates, $Al[CH_2(OH)_2]$ and –OH fragments.

Another fragment $-AlCH_2(O_2)H$ is a quasi-alcohol (analogous to reaction **F**) formed when an O_2 molecule inserts into a C-H bond as a peroxide $(O_2)^{2-}$ with an O-O bond length of 1.47 Å. However no densification is observed, apparently because no surface Al-C bonds are broken.

With eight singlet oxygen atoms reacting with MS in reaction **M**, different surface intermediates are formed. As seen from Figure 5, some ^1O atoms either inserted into C-H bonds of the ligand or into Al-C. The reaction energy is -7.12 eV/^1O (Table 2, reaction **M**). H_2O is the only by-product that desorbs spontaneously in this case at a cost of 0.28 eV. Surface fragments left after the reaction are two formates, -Al(OCHO), along with lossely adsorbed methanediol, $–Al(OH)CH_2OH$ with Al-O of 2.02 Å (as reaction **K**) and –OH. These

fragments show that one ^1O atom inserted into each Al-C bond at the surface. One Al stays 4-coordinated, while the remaining two Al become 4-coordinated and 5-coordinated.

3.1.2 Thermodynamics of each by-product

A variety of by-products were formed simultaneously in many of the reactions described above, which obscures any tendencies for one by-product to be more thermodynamically favoured than another. We therefore examined the overall reaction energy for the exclusive production of each of the four key by-products from our calculations and the literature, spanning the range of oxidation states, namely C_2H_4, CH_2O, CO and CO_2, along with a hydroxylated surface and gas-phase H_2O where necessary. The results are presented in Table 3. It is clear that the more that a C atom is oxidized, the more energy is released. However, the exothermicity per oxygen atom is nearly constant at -7.0±0.4 eV/O regardless of by-product. This suggests that thermodynamics alone does not favour any one of these by-products over the others during O adsorption.

Table 3: Comparing total reaction energies (ΔE) in eV relative to ^1O density and the number of C oxidized in MS for a selection of gaseous by-products proposed from our calculations and in the literature.

Reaction	**Δ*E* (eV/^{1}O)**	**Δ*E* (eV/C)**
$\|\text{--}(AlCH_3)_3 + 3\,^1O \rightarrow \|\text{--}(AlOH)_3 + 3/2C_2H_4$	-7.41	-7.41
$\|\text{--}(AlCH_3)_3 + 6\,^1O \rightarrow \|\text{--}(AlOH)_3 + 3CH_2O$	-6.61	-13.23
$\|\text{--}(AlCH_3)_3 + 9\,^1O \rightarrow \|\text{--}(AlOH)_3 + 3CO + 3H_2O$	-6.59	-19.77
$\|\text{--}(AlCH_3)_3 + 12\,^1O \rightarrow \|\text{--}(AlOH)_3 + 3CO_2 + 3H_2O$	-6.91	-27.63

4. Discussion

We have used DFT to determine the immediate products of the reactive adsorption of various ^1O plasma concentrations onto a methylated alumina surface. Our initial substrate, **MS**, was covered with three $AlCH_3$ fragments per cell and was exposed to various concentrations of ^1O atoms. We find that a wide variety of barrierless reactions can take place, depending on the direction of approach and concentration of ^1O, with spontaneous production of by-products and various surface fragments from the incomplete combustion of the $–CH_3$ ligands. Neutral products may desorb immediately as by-product molecules, whereas anionic products are expected to bind to the alumina surface as intermediates, at least initially. We are interested to find out how much oxidation of C takes place and so the corresponding oxidation states of C are reported in Table 4.

Table 4: Oxidation state of C, denoted *Q*(C), in the by-products and surface intermediates produced during the oxidation of $–CH_3$ by ^1O atoms from O_2 plasma or O_3.

Gaseous by-product	**Surface-bound anion**	***Q*(C)**
CH_4	CH_3^-	-4
C_2H_4, CH_3OH, $CH_3(O_2)H$	CH_3O^-, $CH_2(OH)^-$, $CH_2(O_2)H^-$	-2
CH_3OCH_2OH		-1
CH_2O, $CH_2(OH)_2$	CHO^-, $CH_2O_2^{2-}$	0
CO, HCOOH	$OCHO^-$	2
CO_2	HCO_3^-, $HCO_2(O_2)^-$	4

A key mechanistic question is the identity of the reaction by-product. In the reactions with ^1O atoms investigated here, various neutral by-products were spontaneously formed and could be desorbed from the simulation cell. These by-products are H_2, O_2, CO, H_2O, H_2O_2,

CH_2O, HCOOH, $CH_2(OH)_2$, CH_3OH and CH_3OCH_2OH. The energies required to desorb these by-products are reported in Table 2 and give an indication of volatility. Substantial kinetic energy is released by the reaction (4-8 eV/^{1}O) and we therefore assume that moderate desorption energies (<1 eV/cell) can be rapidly overcome, so that the molecules move away from the surface before reacting further with ^{1}O. Subsequent gas-phase reactions with ^{1}O or other plasma constituents are of course possible during the course of an ALD experiment, so that some of the by-products that we observe may not finally be detected.

We deliberately restrict this study to the cascade of barrierless reactions that occur directly due to the adsorption of ^{1}O atoms. The advantage of this approach is the certainty that these reactions will take place regardless of the actual process temperature. Clearly however, we cannot form concrete conclusions about the temperature-dependent kinetics of subsequent reactions over the experimental timescale and about the resulting product distribution.

Hydroxyl, water and hydrogen peroxide

The hydroxyl group, surf-Al(OH), is the most frequently observed surface intermediate in our simulations, the immediate result of ^{1}O adsorption in seven of the twelve cases presented here. This verifies the original proposal from a more limited theoretical study[21] and the subsequent experimental detection of CH_4 during the TMA pulse signalling that OH groups had been formed in the previous O_2-plasma pulse.[23]

Regardless of the detail of the redox reaction, the production of surf-OH is a straightforward consequence of the conservation of atoms and charge. Firstly, the neutral organic by-products all have even numbers of H atoms, whereas the methyl reactant has an odd number, so that one H remains at the surface when the by-product desorbs. Secondly, neutral by-products can desorb, but the formal negative charge on the methyl reactant must remain on the surface in the form of another anionic intermediate. In reaction **C**, with just one ^{1}O

available for oxidation, the surface intermediate that meets these criteria is the hydride anion. In reaction **E**, and most other simulations where at least two ^{1}O atoms per methyl group are available, surface OH is produced.

As for thermal ALD then, the amount of Al deposited in each ALD cycle depends linearly on the coverage of surf-OH at the end of the O-reagent pulse, and thus on the coverage of methyl groups available for oxidation after the TMA pulse. The consequences for the rate of ALD growth are outlined in Elliott *et al.*[21] and Elliott & Nilsen[44].

In two O-rich cases (reactions **M** and **O**) we observed the spontaneous reaction of ^{1}O with two adjacent methyl H's, which resulted in desorption of H_2O as by-product in the case of reaction **O**. Further oxidation to hydrogen peroxide, H_2O_2, was observed in two further cases (reactions **H** and **L**).

Since hydroxyl groups are produced so readily during oxidation, we should consider the possibility of them combining and desorbing as water according to

$$\text{surf-Al(OH)} + \text{surf-Al(OH)} \rightarrow H_2O_{(g)} + \text{surf-Al-O-Al} \qquad (1)$$

The barrier to this reaction is likely to be overcome via thermal activation over the experimental timescale, perhaps as a result of the high exothermicity of the redox reactions. Quantifying this would require a proper study of proton diffusion across the surface, which is beyond the current scope.

It has been proposed in the literature[22] that re-adsorption of the H_2O product could be the source of surf-OH, the reverse of reaction (1). However, DFT calculations[28] and sensitive vibrational spectroscopy[17] have shown that a substantial barrier can prevent H_2O from adsorbing to individual Al atoms at the surface at low temperature. H_2O re-adsorption was not observed in our simulations, but of course could occur over longer timescales, especially

if H_2O is a product of secondary oxidation of other by-products in the gas phase. Nevertheless, we find it reasonable on statistical grounds to assert that the main source of surf-OH is the original oxidation reaction that produces OH, rather than subsequent combination, desorption and re-adsorption reactions.

Depending on the rate of surface proton diffusion, protons from OH groups may also associate with other anionic intermediates into neutral by-products, which may then desorb, as discussed below. The result will be a lower coverage of OH groups and a partially bare Al_2O_3 surface. It has been computed that TMA dissociatively chemisorbs onto bare Al and O sites, leading again to saturation of the surface with methyl groups, but also to a lower ALD growth rate.[12]

Methanol and ethene

By-products resembling methanol or intermediates in methanol formation are also observed in a few simulations: neutral CH_3OH (reaction **J**), anionic surf–OCH_3 (reaction **D**), surf–CH_2OH (reaction **F**) and the peroxo derivative surf–$CH_2(O_2)H$ (reaction **L**) all showing Q(C)=-2. A related ether by-product with overall Q(C)=-1 also results from ^{1}O oxidation (CH_3OCH_2OH, reaction **I**).

Dehydration of two methanol molecules would in principle produce ethene, C_2H_4, also with Q(C)=-2. An alternative route to ethene via high-spin coupling of two surface-CH_2 species was proposed in a previous theoretical study.[21] Both reactions would require thermal activation and neither reaction was observed in our optimizations. Nevertheless we note that, in principle, a C_2H_4 by-product would leave behind a hydroxylated surface, while the CH_3OH by-product would leave a bare alumina surface.

As polar molecules, these neutral alcohols show fairly strong adhesion to the surface, with desorption energies of 0.55 and 0.95 eV for CH_3OH and CH_3OCH_2OH respectively. Under thermal ALD conditions such by-products could be expected to occupy adsorption sites, hindering further precursor adsorption and lowering the growth rate. However here we suggest that the exothermicity of the oxidation reaction will deliver enough energy locally for desorption to take place.

Furthermore, even when oxidation has finished, we expect that there will be continual transfer of energy from the plasma to the surface as oxygen atoms or ions collide with the surface and recombine into O_2. Thermally-induced desorption of all neutral species may therefore be expected over the second-long timescale of the O-plasma pulse. We speculate that there are fewer reactive gas-phase species when ozone is used as oxidant and that this cleaning effect may consequently be less pronounced in the ozone process than in the O_2-plasma process. Cleaning off weakly-bound by-products may thus explain the higher growth rate for O_2-plasma relative to ozone.

Formaldehyde

We find formaldehyde, CH_2O, to be the most frequently observed by-product, occurring in over half of the reactions shown in Table 2 - mostly as an unbound neutral molecule (reactions **C**, **E**, **F** and **K**), but also binding to under-coordinated surface Al as a neutral molecule (**I** and **J**) or anion (**L**). The unbound molecule shows a desorption energy in the range 0.05-0.35 eV, indicating that it is volatile. The formal oxidation state of C in CH_2O is Q(C)=0. Of all the oxidation reactions that we observed, those producing CH_2O are not the most thermodynamically favourable (*e.g.* ΔE=-4.99 eV/^{1}O for reaction **C** with surface intermediate Al-H or ΔE=-6.76 eV/^{1}O for reaction **E** with Al-OH) but seem to be the most kinetically accessible and most frequently sampled, particularly at low ^{1}O concentration. Our

simulations show that gas-phase ^1O atoms can approach surface-bound methyl groups, insert into a C-H bond and produce CH_2O without any kinetic barrier.

Methanediol, $CH_2(OH)_2$, is observed as a bound dianion (reaction **J**) and as a neutral bound molecule (reaction **M**). This by-product may be considered as the hydrated form of formaldehyde, *i.e.* $CH_2O+H_2O=CH_2(OH)_2$, and so has C in the same oxidation state, $Q(C)=0$. A by-product with $Q(C)=0$ is thus formed in two-thirds of the reactions detailed in Table 2.

Formate and formic acid

Formate (surf-$OCHO^-$) is assigned as the primary surface intermediate detected with IR by Chabal *et al.*[24] Consistent with this, our simulations include some cases where high ^1O concentrations result in immediate oxidation to formate (reactions **H**, **J** and **M**). For this reaction, at least three ^1O are required per methyl group, with two of them inserting into C-H bonds, resulting in oxidation state $q(C)=+2$. Decomposition products with C in the same oxidation state, $CO+H_2O$, are also observed as the products of reaction **O**.

Carbonate and carbon dioxide

It is appealing to assume that O_2-plasma and ozone are such strong oxidizing agents that they completely combust organic ligands (such as methyl) to CO_2, with $Q(C)=+4$. This by-product is not observed in our simulations. However related anions with $Q(C)=+4$ are seen as immediate products in the most O-rich case (reaction **O**): hydrogencarbonate, HCO_3^- (also known as bicarbonate), and a version with oxide replaced by peroxide, $HCO_2(O_2)^-$. The mechanism for formation of the hydrogencarbonates again involves the spontaneous insertion of O or O_2 into C-H bonds of the ligand. Protonation of these anions would presumably lead to desorption of CO_2, along with H_2O or H_2O_2.

Densification

We monitored Al-O coordination during the oxidation process in our simulations and observed densification of some surface Al in reactions **I**, **J**, **K**, **M** and **O** in Table 2. We checked when an Al-O bond was formed by comparing to the range of bond lengths in the bulk (Al-O=1.85–2.01 Å). We identified two situations that lead to densification. Firstly, Al can form new bonds to surface fragments such as hydroxyl, formate or carbonate. For instance, the coordination number (c.n.) of some surface Al increased from four to five in reactions **I** (Al-O=1.7-2.12 Å), **J** (Al-O=1.87– 2.0 Å), **M** (Al-O=1.89-2.02 Å) and **O** (Al-O=1.76-2.07 Å). Secondly, our calculations show that complete loss of a methyl ligand also leads to densification, freeing up surface Al to bond to bulk O in the layer below. This is observed in reactions **J** (c.n.=5) and **K** (c.n=4, Al-O=1.82 Å), but not in reaction **I** because Al remains bonded to other surface fragments.

We therefore suggest that Al/O coordination numbers will increase as chemically-bound ligands are replaced with oxidised fragments on the surface during this ALD pulse. In particular, reactions that generate a bare surface during the ALD process should lead to a more dense metal oxide film.

Self-limiting chemistry

It is clear from the results in Table 2 that O_2-plasma removes carbon efficiently from the methylated surface even at low concentrations of the ^{1}O reactant. As discussed above, a range of by-products and surface intermediates is likely to be formed, with higher oxidation states possible at higher ^{1}O concentration. All reactions are strongly exothermic, with little difference between the various by-products in terms of the energy released per oxygen atom (Table 3). However, it is interesting to note that products with the oxidation state Q(C)=0, such as CH_2O, are apparently most favoured *kinetically*, regardless of the concentration of incident oxygen atoms. This is evident in the distribution of Q(C) for by-products that is

shown in Figure 6. Desorption of by-products from the surface means that carbon is no longer available for oxidation and this is one way that the reaction with ^{1}O self-limits.

However, not all the carbon is observed to desorb spontaneously, with a proportion remaining for longer timescales within surface-bound intermediates. The evolution of the overall oxidation state of the surface with ^{1}O concentration is therefore also examined in Figure 6. The progressive oxidation of surface fragments with oxygen concentration is apparent, but not reaching the maximum oxidation state Q(C)=+4. Instead, excess ^{1}O reacts with oxygen rather than carbon, resulting in O_2 (reaction **L**), or related peroxo-based compounds H_2O_2 (reactions **H** and **L**), $CH_2(O_2)H$ (reaction **L**) and $HCO_2(O_2)^-$ (reaction **O**). This indicates that the gas-surface reaction self-limits kinetically through exhaustion of the capacity of the surface to become oxidized, even when carbon is still present.

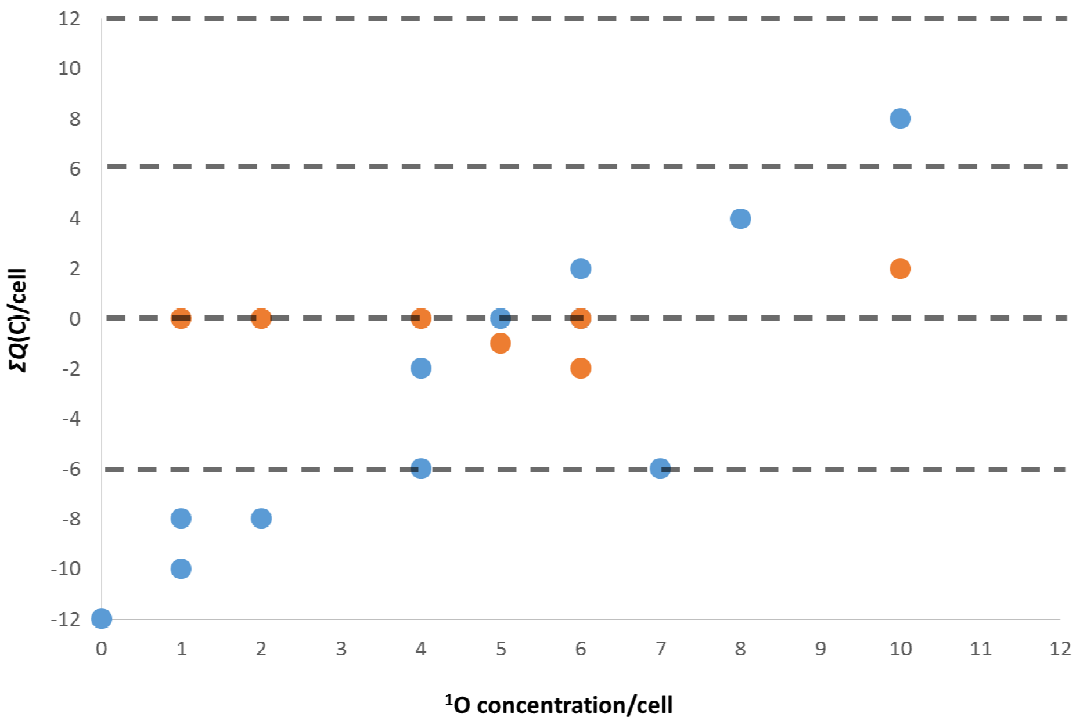

Figure 6: Simulated saturation curve for O_2-plasma or ozone ALD pulse, showing total oxidation state of C, ΣQ(C), in surface-bound intermediates (blue) and gas-phase by-products (orange) as a function of ^{1}O concentration (data from Table 2). Dashed horizontal lines show the formal oxidation states of the main by-products (Table 4).

We are thus able to determine the capacity for the methylated surface to become oxidized in the O_2-plasma or ozone ALD pulse. The minimum amount of reactant would be one ^1O per methyl group according to:

$$\text{surf-}CH_3 + {}^1O_{(g)} \rightarrow \tfrac{1}{2}.C_2H_{4\,(g)} + \text{surf-OH.} \qquad (2)$$

The theoretical maximum would be four times higher:

$$\text{surf-}CH_3 + 4({}^1O)_{(g)} \rightarrow CO_{2\,(g)} + H_2O_{(g)} + \text{surf-OH.} \qquad (3)$$

Our data indicate that saturation of the redox reaction occurs at the intermediate level $Q(C)=0$, transferring four electrons per C atom and thus requiring two ^1O per CH_3 group. For the **MS** model, this means an incident ^1O flux of 0.4 atoms/nm^2. The most likely reaction is:

$$\text{surf-}CH_3 + 2({}^1O)_{(g)} \rightarrow CH_2O_{(g)} + \text{surf-OH.} \qquad (4)$$

Conclusion

The aim of this study was to investigate the plausible reaction mechanisms, surface intermediates and by-products formed when a remote O_2-plasma or O_3 is used as oxygen source in the ALD of alumina. Our approach was to examine the sequence of reactions immediately following oxygen adsorption onto the methylated surface that is typically present when trimethylaluminium is used as Al precursor. We did this by using DFT to optimise geometries containing different concentrations of neutral ^1O atoms approaching the CH_3-covered surface. The main outcome is that a wide variety of barrierless and exothermic reactions can take place in which the surface carbon is oxidised and, in many of these cases,

the gaseous by-products and surface-bound intermediates that are spontaneously formed are indicative of a self-limiting surface chemistry, as required for ALD.

The simulations reveal the spontaneous production of by-products with enough kinetic energy to overcome their relatively low desorption energies. As each oxygen atom reaches the surface and reacts, there is no thermodynamic driving force favouring one by-product over any other. However formaldehyde, CH_2O, is the most frequently observed gaseous by-product, apparently favoured by kinetics. Desorption of this by-product leads to saturation of the redox reaction at the level of two singlet oxygen atoms per CH_3 group, rather than further reaction with oxygen to higher oxidation states of carbon. Other oxidation states are possible, yielding the by-products CH_3OH, $CH_2(OH)_2$ and CO, as well as CO_2 if surface carbonates decompose. The self-limiting chemistry that defines ALD thus comes about through the kinetically-driven desorption of oxidisable carbon from the surface prior to complete oxidation.

The hydroxyl (OH) group is the most frequently observed intermediate that remains bound to the surface after oxidation, consistent with its reactivity towards TMA in the next ALD cycle. It is formed directly in the simulations when a methyl ligand is initially oxidized, rather than from subsequent combination, desorption and re-adsorption of molecular water, as has been previously suggested. Other anionic intermediates such as formates are also commonly observed in the simulations. However it is worth emphasising that other constituents of O_2-plasma, such as triplet spin states or molecules, could produce different surface intermediates and by-products.

We monitored how the oxidation of ligands affected the densification of Al and O into bulk-like environments. The simulations suggest that Al/O coordination numbers in the final film increase during the ALD pulse as methyl ligands are removed or are replaced with oxidised

fragments. These are some of the first indications of how growth chemistry affects film morphology in metal oxide ALD, but more work is clearly needed on this complex topic.

Acknowledgements

This research received funding from the European Union's Seventh Framework Programme for research, technological development and demonstration under grant agreement number 606889; project ESR-2 in the framework of the RAPID (Reactive Atmospheric Plasma processIng – eDucation network) Marie Curie Initial Training Network (http://www.rapid-itn.eu). The authors acknowledge the DJEI/DES/SFI/HEA Irish Center for High-End Computing (ICHEC) for the provision of computational facilities and support.

References

[1] T. Suntola, J. Antson, *Method for Producing Compound Thin Films*, **1977**, US 4 058430.

[2] H. B. Profijt, S. E. Potts, M. C. M. van de Sanden, W. M. M. Kessels, *J. Vac. Sci. Technol. A Vacuum, Surfaces, Film.* **2011**, *29*, 050801.

[3] E. Langereis, S. B. S. Heil, M. C. M. van de Sanden, W. M. M. Kessels, *J. Appl. Phys.* **2006**, *100*, 023534.

[4] van de Sanden, van de, S. B. S Heil, E. Langereis, A. Kemmeren, F. Roozeboom, M. C. M van de Sanden, W. M. M Kessels, **2005**, DOI 10.1116/1.1938981.

[5] A. Rahtu, T. Alaranta, M. Ritala, *Langmuir* **2001**, *17*, 6506.

[6] P. W. Loscutoff, H. Zhou, S. B. Clendenning, S. F. Bent, *ACS Nano* **2010**, *4*, 331.

[7] S. B. S. Heil, P. Kudlacek, E. Langereis, R. Engeln, M. C. M. van de Sanden, W. M. M. Kessels, *Appl. Phys. Lett.* **2006**, *89*, 131505.

[8] S. B. S. Heil, J. L. van Hemmen, C. J. Hodson, N. Singh, J. H. Klootwijk, F. Roozeboom, M. C. M. van de Sanden, W. M. M. Kessels, *J. Vac. Sci. Technol. A Vacuum, Surfaces, Film.* **2007**, *25*, 1357.

[9] B. Hoex, S. B. S. Heil, E. Langereis, M. C. M. van de Sanden, W. M. M. Kessels, *Appl. Phys. Lett.* **2006**, *89*, 042112.

[10] H.-L. Lu, W. Chen, S.-J. Ding, M. Xu, D. W. Zhang, L.-K. Wang, *J. Phys. Condens. Matter* **2005**, *17*, 7517.

[11] T. Weckman, K. Laasonen, *Phys. Chem. Chem. Phys.* **2015**, *17*, 17322.

[12] S. D. Elliott, J. C. Greer, *J. Mater. Chem.* **2004**, *14*, 3246.

[13] S. D. Elliott, G. Dey, Y. Maimaiti, H. Ablat, E. A. Filatova, G. N. Fomengia, *Adv. Mater.* **2015**, n/a.

[14] V. R. Rai, V. Vandalon, S. Agarwal, *Langmuir* **2012**, *28*, 350.

[15] J. Musschoot, J. Dendooven, D. Deduytsche, J. Haemers, G. Buyle, C. Detavernier, *Surf. Coatings Technol.* **2012**, *206*, 4511.

[16] V. Verlaan, L. R. J. G. van den Elzen, G. Dingemans, M. C. M. van de Sanden, W. M. M. Kessels, *Phys. status solidi* **2010**, NA.

[17] V. Vandalon, W. M. M. Kessels, *Appl. Phys. Lett.* **2016**, *108*, 011607.

[18] J. L. van Hemmen, S. B. S. Heil, J. H. Klootwijk, F. Roozeboom, C. J. Hodson, M. C. M. van de Sanden, W. M. M. Kessels, *J. Electrochem. Soc.* **2007**, *154*, G165.

[19] S. K. Kim, S. W. Lee, C. S. Hwang, Y.-S. Min, J. Y. Won, J. Jeong, *J. Electrochem. Soc.* **2006**, *153*, F69.

[20] † M. D. Groner, † F. H. Fabreguette, † and J. W. Elam, †,‡ S. M. George*, **2004**, DOI 10.1021/CM0304546.

[21] S. D. Elliott, G. Scarel, C. Wiemer, M. Fanciulli, G. Pavia, *Chem. Mater.* **2006**, *18*, 3764.

[22] S. B. S. Heil, J. L. van Hemmen, M. C. M. van de Sanden, W. M. M. Kessels, *J. Appl. Phys.* **2008**, *103*, 103302.

[23] S. B. S. Heil, P. Kudlacek, E. Langereis, R. Engeln, M. C. M. van de Sanden, W. M. M. Kessels, *Appl. Phys. Lett.* **2006**, *89*, 131505.

[24] J. Kwon, M. Dai, M. D. Halls, Y. J. Chabal, *Chem. Mater.* **2008**, *20*, 3248.

[25] V. R. Rai, V. Vandalon, S. Agarwal, *Langmuir* **2010**, *26*, 13732.

[26] E. Langereis, J. Keijmel, M. C. M. van de Sanden, W. M. M. Kessels, *Appl. Phys. Lett.* **2008**, *92*, 231904.

[27] C. Mastai, C. Lanthony, S. Olivier, J.-M. Ducéré, G. Landa, A. Estève, M. Djafari Rouhani, N. Richard, A. Dkhissi, **n.d.**, DOI 10.1016/j.tsf.2011.10.125.

[28] M. Shirazi, S. D. Elliott, *Nanoscale* **2015**, *7*, 6311.

[29] R. L. Puurunen, *J. Appl. Phys.* **2005**, *97*, 121301.

[30] Z. Łodziana and J. K. Nørskov, "The stability of the hydroxylated „0001… surface of a-Al2O3," DOI 10.1063/1.1574798#can be found under http://orbit.dtu.dk/fedora/objects/orbit:18715/datastreams/file_4287231/content, **n.d.**

[31] H. B. Profijt, M. C. M. ; ; Van De Sanden, W. M. M. Kessels, M. C. M. Van De Sanden, **2013**, DOI DOI:10.1116/1.4756906.

[32] G.-Y. Fang, L.-N. Xu, Y.-Q. Cao, L.-G. Wang, D. Wu, A.-D. Li, *Chem. Commun.* **2015**, *51*, 1341.

[33] Y. Jeong, S. Baek, D. Kim, J. Kim, Y. Kim, *Appl. Surf. Sci.* **2013**, *280*, 207.

[34] S. Tinck, A. Bogaerts, *Plasma Sources Sci. Technol.* **2011**, *20*, 015008.

[35] G. Kresse, J. Furthmüller, *Phys. Rev. B* **1996**, *54*, 11169.

[36] J. P. Perdew, K. Burke, M. Ernzerhof, *Phys. Rev. Lett.* **1996**, *77*, 3865.

[37] P. E. Blöchl, *Phys. Rev. B* **1994**, *50*, 17953.

[38] H. J. Monkhorst, J. D. Pack, *Phys. Rev. B* **1976**, *13*, 5188.

[39] T. Weckman, K. Laasonen, *Phys. Chem. Chem. Phys.* **2015**, *17*, 17322.

[40] A. Heyman, C. B. Musgrave, *J. Phys. Chem. B* **2004**, *108*, 5718.

[41] *Appl. Surf. Sci.* **1996**, *107*, 107.

[42] *,†,‡ Riikka L. Puurunen, §. Andrew Root, ‡,∥ Suvi Haukka, ‡,∇ Eero I. Iiskola, ⊥ and Marina Lindblad, A. O. I. Krause†, **2000**, DOI 10.1021/JP000454I.

[43] G. Prechtl, a. Kersch, G. S. Icking-Konert, W. Jacobs, T. Hecht, H. Boubekeur, U. Schroder, *IEEE Int. Electron Devices Meet. 2003* **2003**, 3.

[44] S. D. Elliott, O. Nilsen, in *ECS Trans.*, The Electrochemical Society, **2011**, pp. 175–183.

Supplementary Information for

First principles mechanistic study of self-limiting oxidative adsorption of remote oxygen plasma during the atomic layer deposition of alumina

by Glen N. Fomengia, Michael Nolan, Simon D. Elliott

These supplementary figures show initial geometries prior to DFT optimization, generated by introducing various concentrations of singlet oxygen atoms to the MS model of the methylated surface.

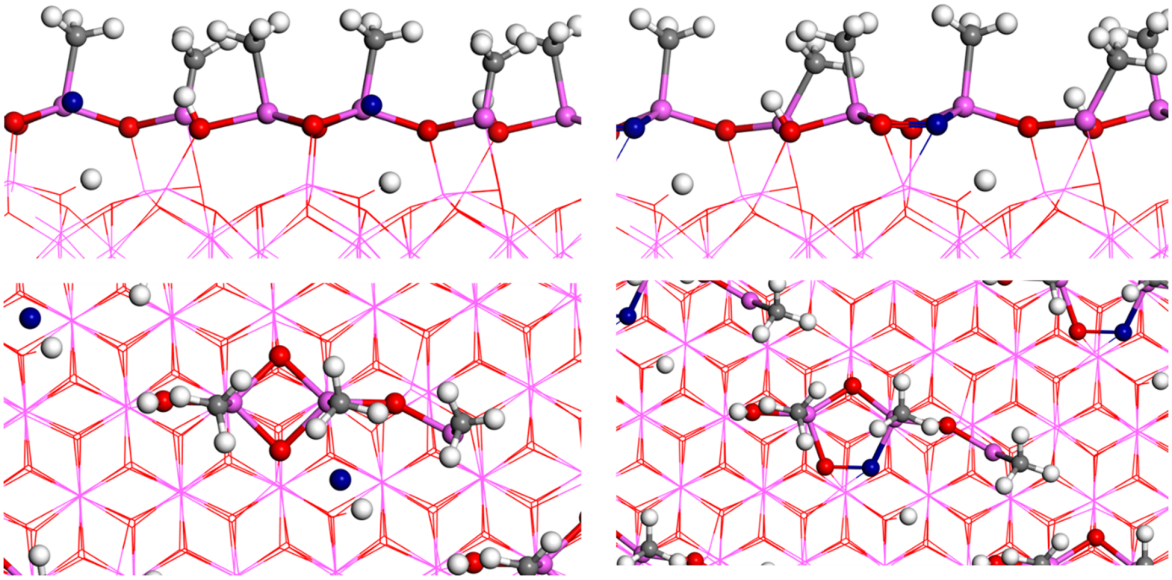

Figure A1: Side and top views showing how a single ^{1}O atom attacks a 4-coordinated surface aluminium atom before relaxation (left panel) and after relaxation (right panel). After relaxation, there is no insertion of ^{1}O into Al-C, rather forming adsorbed peroxide *i.e.* $(O_2)^{2-}$ with computed O-O bond length = 1.53 Å.

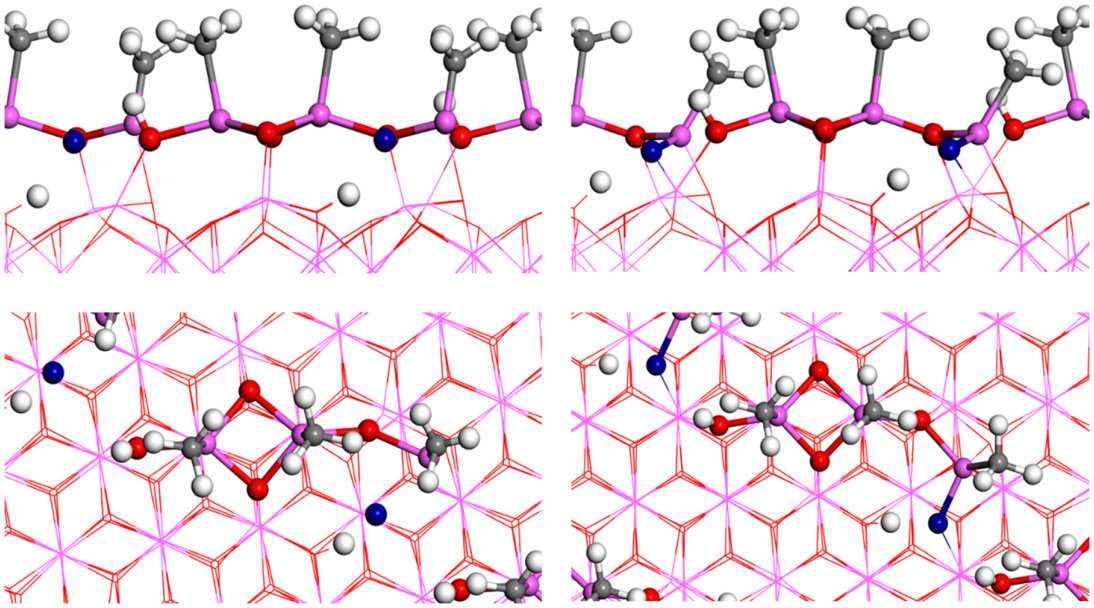

Figure A2: Side and top views showing how a single ^{1}O atom attacks a 4-coordinated surface aluminium atom before relaxation (left panel) and after relaxation (right panel). After relaxation, there is no insertion of ^{1}O into Al-C, rather forming a bridged to Al in the bulk (Al-O-Al).

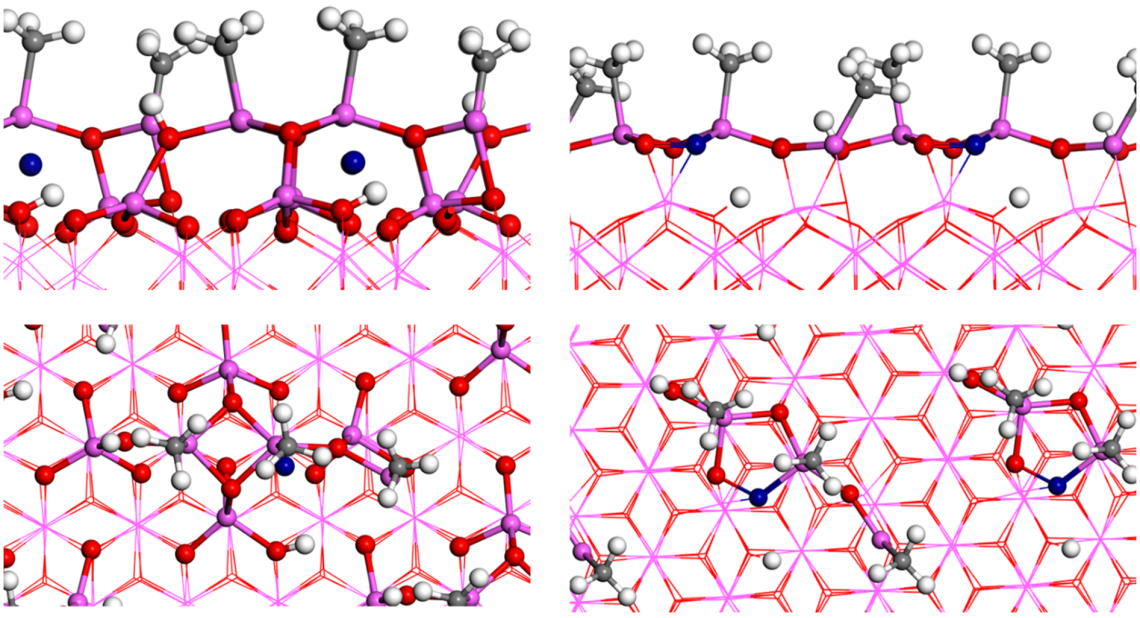

Figure A3: Side and top views showing how a single ^{1}O atom reacts in the subsurface before relaxation (left panel) and after relaxation (right panel). After relaxation, ^{1}O forms a peroxide with a surface oxygen with computed O-O bond length = 1.53 Å.

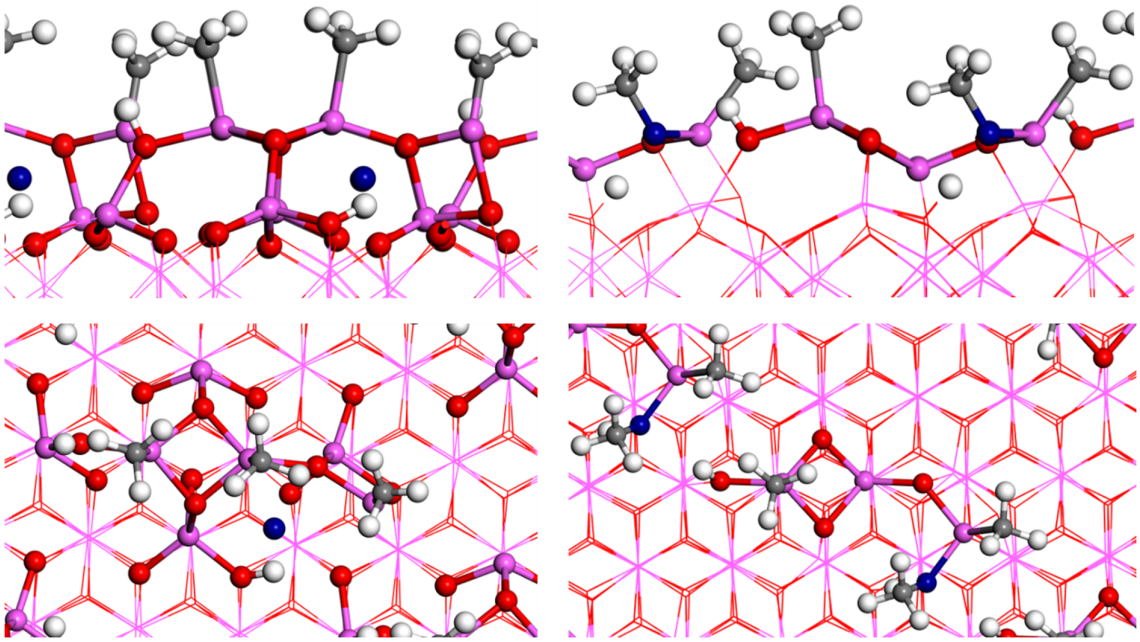

Figure A4: Side and top views showing how a single ^{1}O atom reacts in the subsurface before relaxation (left panel) and after relaxation (right panel). After relaxation, ^{1}O inserts between Al-C bond to form $–OCH_3$, as in reaction D.

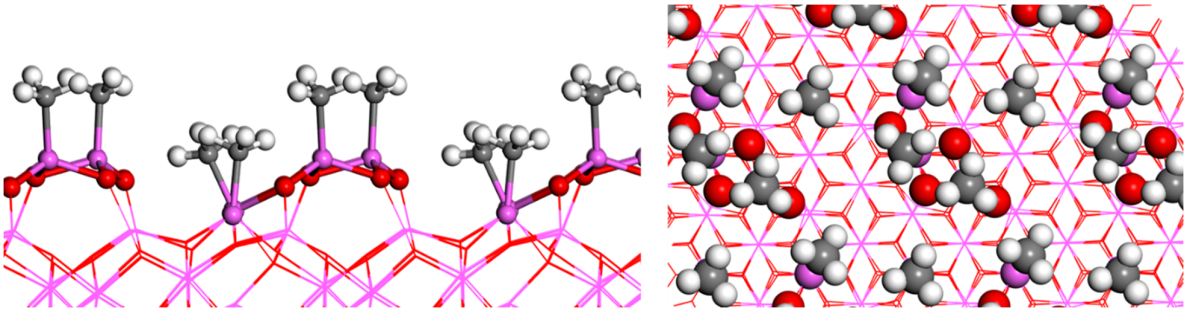

Figure B1: Side and top view of the four $AlCH_3$ fragments on the surface after the adsorption of 4 TMA with subsequent desorption of 8 CH_4. This geometry is used for relaxation in reaction B^*, Table 1.

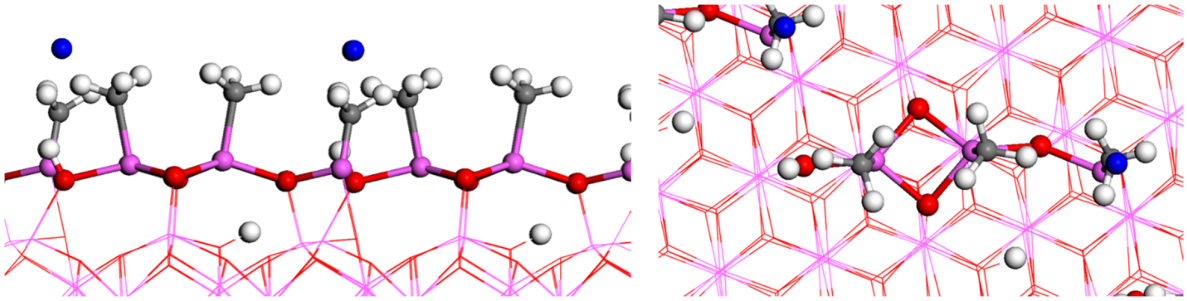

Figure C1: Side (left panel) and top (right panel) views prior to relaxation of a single ^{1}O approaching the carbon atom of the methyl ligand from the top. This geometry is used for relaxation in reaction C, Table 2.

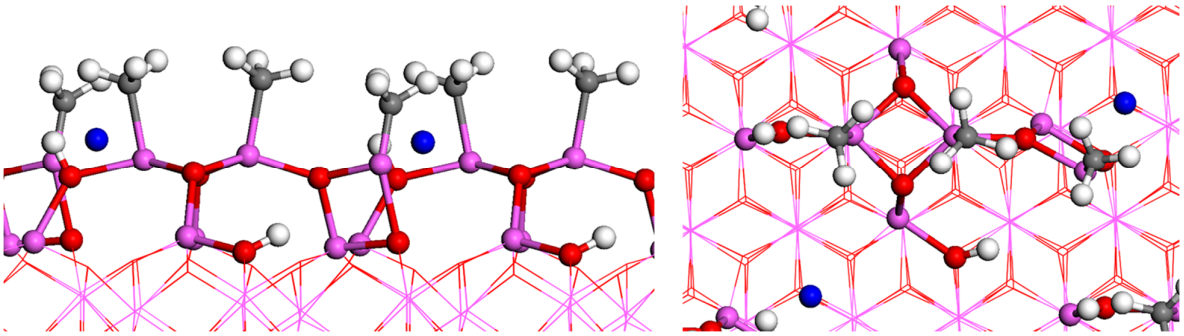

Figure D1: Side (left panel) and top (right panel) views prior to relaxation of a single ^{1}O approaching a surface aluminium atom from the side. This geometry is used for relaxation in reaction D, Table 2.

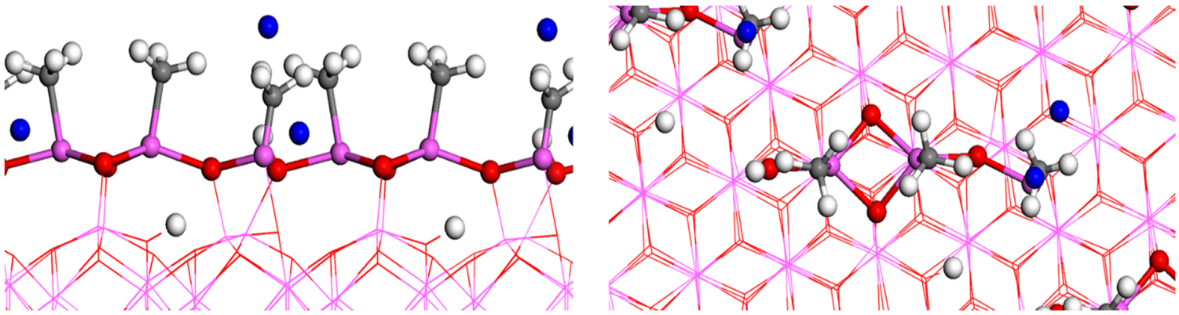

Figure E1: Side (left panel) and top (right panel) views of surface models of oxidation of MS with two ^{1}O prior to relaxation. This geometry is used for relaxation in reaction E, Table 2.

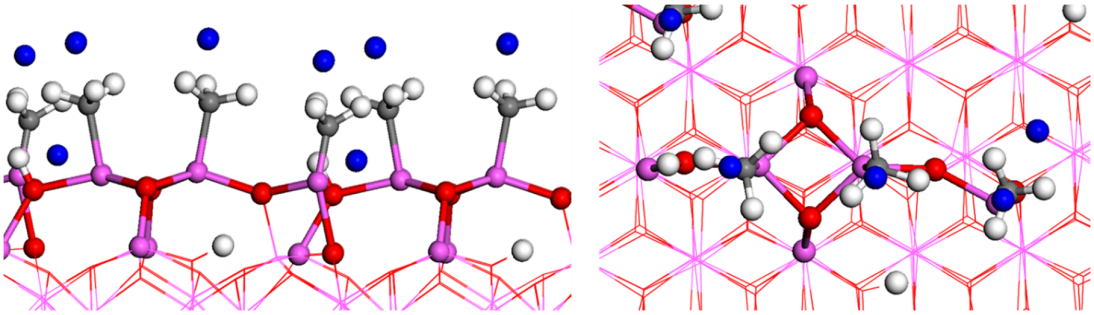

Figure F1: Side (left panel) and top (right panel) views of surface models of oxidation of MS with four ^{1}O prior to relaxation. Three of these ^{1}O atoms attack the ligand from the top while the remaining one attacks surface aluminium from the side. This geometry is used for relaxation in reaction F, Table 2.

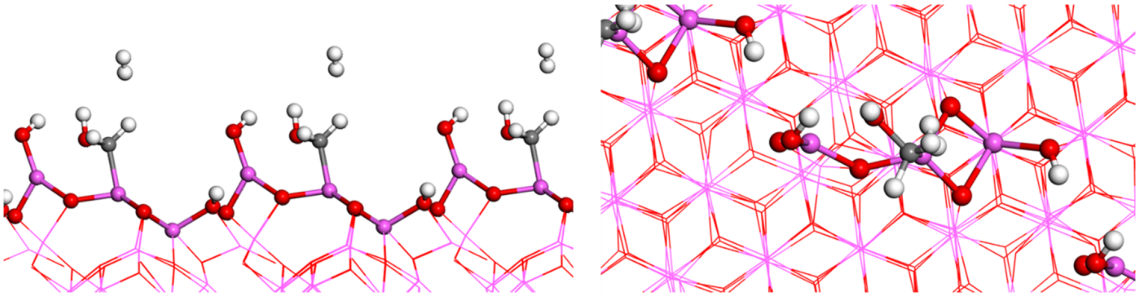

Figure F2: Short DFT-based MD simulations from the same initial geometry as F at 423 K spontaneously produced the same by-products and surface fragments. However, H^- that was weakly bonded to Al in reaction F, Table 2, combined with a nearby proton in the subsurface layer to produce H_2, as shown here in the final geometry from the MD simulation.

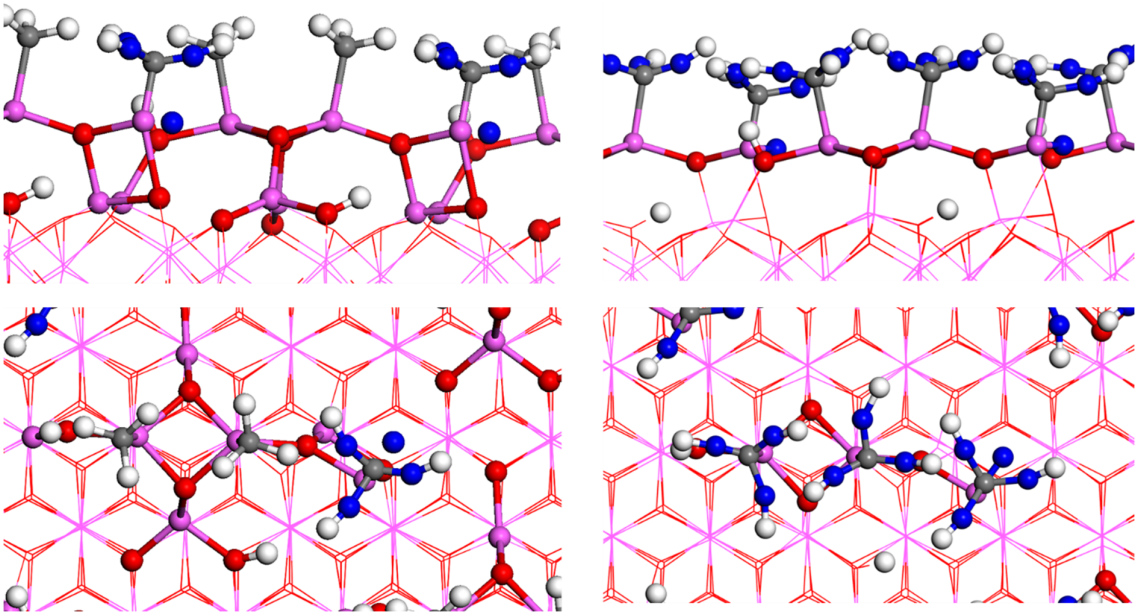

Figure H1: Side and top views of surface before geometry optimisation of MS with three ^{1}O atoms (left panel) and nine ^{1}O atoms (right panel) inserted into multiple C-H bonds. These geometries are used respectively for relaxation in reaction H and O, Table 2.

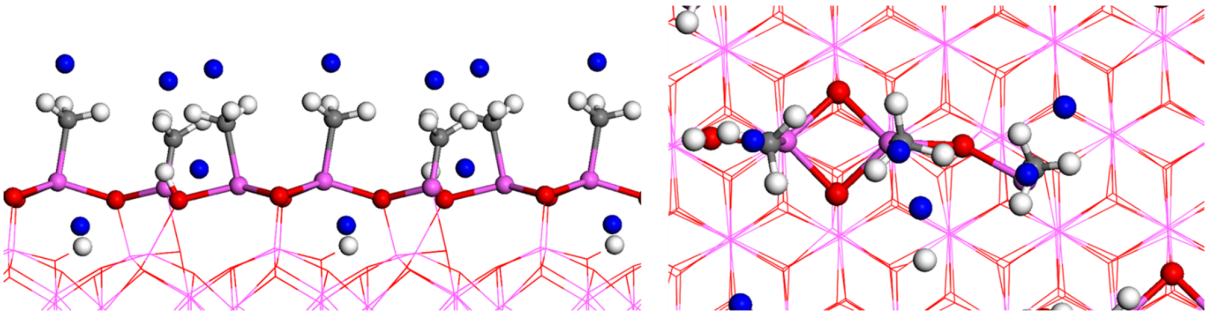

Figure I1: Side (left panel) and top (right panel) views of surface models of oxidation of MS with five ^{1}O prior to relaxation. This geometry is used for relaxation in reaction I, Table 2.

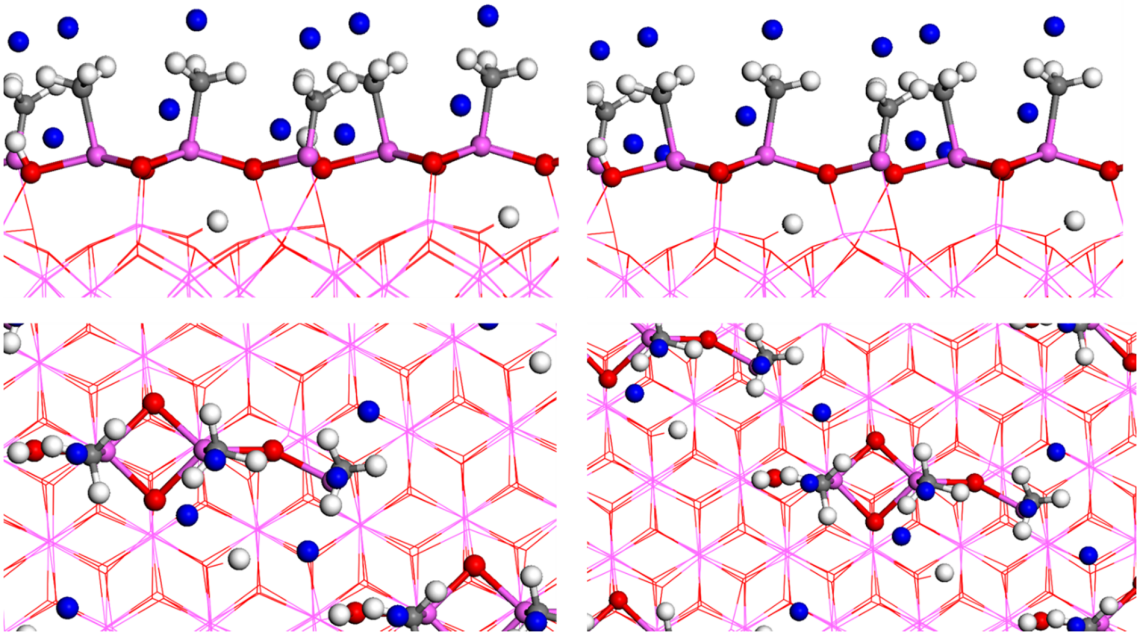

Figure J1: Side and top views of two surface before geometry optimisation of MS with six ^{1}O atoms in different positions. After relaxation, CH_3OH (left panel) while two CH_2O (right panel) were produced spontaneously. The structure in the right was used as the initial geometry to determine the total reaction energy, generating 3OH groups on the surface as seen in Figure G.

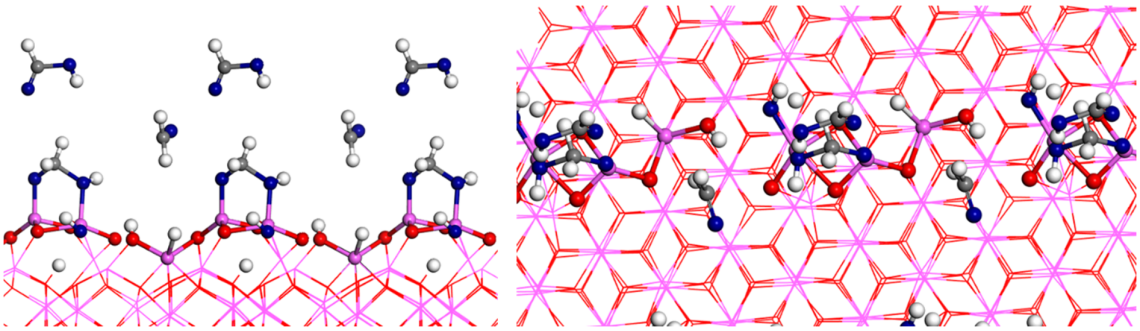

Figure J2: Side (left panel) and top (right panel) views of surface after short DFT-MD runs. The initial geometry in structure J1 (left panel) was used for this run producing CH_2O and HCOOH as by-products.

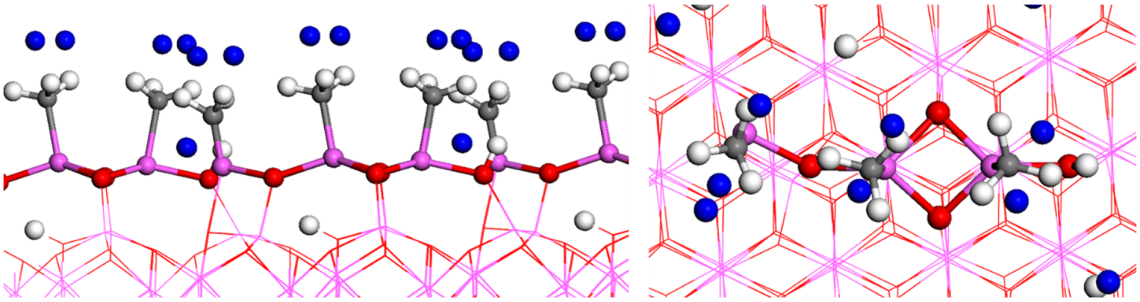

Figure L1: Side (left panel) and top (right panel) views of surface models of oxidation of MS with seven ^{1}O prior to relaxation. This geometry is used for relaxation in reaction L, Table 2.

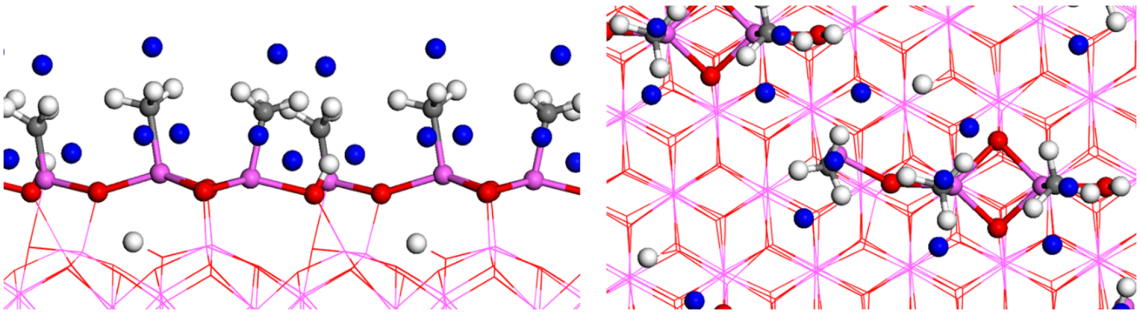

Figure M1: Side (left panel) and top (right panel) views of surface models of oxidation of MS with eight ^{1}O prior to relaxation. This geometry is used for relaxation in reaction M, Table 2.